JOURNAL OF PETROLOGY | VOLUME 43 | NUMBER 3 | PAGES 449–484 | 2002

Basement Geochemistry and Geochronology of Central Malaita, Solomon Islands, with Implications for the Origin and Evolution of the Ontong Java Plateau

M. L. G. TEJADA[1]*, J. J. MAHONEY[2], C. R. NEAL[3], R. A. DUNCAN[4] AND M. G. PETTERSON[5]

[1]NATIONAL INSTITUTE OF GEOLOGICAL SCIENCES, UNIVERSITY OF THE PHILIPPINES, DILIMAN, QUEZON CITY, 1101 PHILIPPINES

[2]SCHOOL OF OCEAN AND EARTH SCIENCE AND TECHNOLOGY, UNIVERSITY OF HAWAII, HONOLULU, HI 96822, USA

[3]DEPARTMENT OF CIVIL ENGINEERING AND GEOLOGICAL SCIENCES, UNIVERSITY OF NOTRE DAME, NOTRE DAME, IN 46556, USA

[4]COLLEGE OF OCEANIC AND ATMOSPHERIC SCIENCES, OREGON STATE UNIVERSITY, CORVALLIS, OR 97331, USA

[5]BRITISH GEOLOGICAL SURVEY, ONSHORE MINERALS AND ENERGY RESOURCES, KEYWORTH NG12 5GG, UK

RECEIVED OCTOBER 10, 2000; REVISED TYPESCRIPT ACCEPTED SEPTEMBER 7, 2001

Sections of Ontong Java Plateau basalt basement in central Malaita (Solomon Islands) are 0·5–3·5 km thick and resemble a much-expanded version of that recovered at Ocean Drilling Program Site 807. ^{40}Ar–^{39}Ar ages (121–125 Ma) are identical to those for Site 807, southern Malaita, Ramos Island, parts of the island of Santa Isabel, and Deep Sea Drilling Project Site 289; the ~90 Ma eruptive episode seen in Santa Isabel, San Cristobal, and at drill sites 803 and 288 is not represented. The central Malaitan basalts provide further evidence of two distinct ocean-island-like mantle sources, and the combined data preclude a significant contribution from normal ocean-ridge-type mantle. As at Site 807, two geochemically distinct stratigraphic groups are present, the Singgalo Formation (~750 m thick in central Malaita) and the Kwaimbaita Formation (>2700 m thick). Both a peridotite plume-head and eclogite-bearing plume-head may account for the geochemical characteristics, but the observed stratigraphic succession requires special conditions for the latter model. A number of first-order features of the Ontong Java Plateau do not obviously fit the predictions of any plume-head model: for example, at least two important, geochemically similar eruptive episodes ~30 my apart, the lack of an obvious plume-tail trace, and lack of evidence for emergence or significant uplift.

KEY WORDS: *Ontong Java Plateau; geochemistry; mantle sources; petrogenesis; eruptive stratigraphy*

INTRODUCTION

The Solomon islands of Malaita, Ramos, Ulawa, the northeastern part of Santa Isabel, and probably part of San Cristobal (a.k.a. Makira) form the obducted and uplifted southwestern margin of the world's largest volcanic oceanic plateau, the 5×10^7 km^3 Ontong Java Plateau (OJP; Fig. 1) (e.g. Kroenke, 1972; Hughes & Turner, 1977; Coleman *et al.*, 1978; Coleman & Kroenke, 1981; Petterson *et al.*, 1997; Phinney *et al.*, 1999). Reconnaissance studies show that the Cretaceous igneous basement of these islands is almost indistinguishable in age from, and closely similar in composition to, that drilled at Ocean Drilling Program (ODP) Sites 807 and 803 and Deep Sea Drilling Project (DSDP) Site 289 on the northern and north–central plateau (Mahoney *et al.*, 1993; Parkinson *et al.*, 1996; Tejada *et al.*, 1996; Neal *et al.*, 1997). Recently, we sampled accessible portions of

*Corresponding author. Telephone: 632-435-4837. Fax: 632-929-6047. E-mail: mtejada@nigs.upd.edu.ph

0·5- and 3·5-km-thick sections of OJP crust in central Malaita. As the deepest exposures of the plateau's crust yet sampled systematically, these sections present a unique source of information on age, eruptive stratigraphy, petrogenesis, and mantle sources. In this paper, we characterize the geochemical stratigraphy of the southern OJP crust recorded in these sections, and build upon previous work to examine what the isotopic and chemical variations reveal about the plateau's origin and the implications for the mantle source regions that fed plateau magmatism.

STUDY AREA AND GENERAL FIELD CHARACTERISTICS OF OJP CRUST IN MALAITA

Cretaceous igneous OJP crust forms the cores of several large anticlines in Malaita (Fig. 2a) and is exposed in stream gullies and waterfalls on this heavily vegetated island. The basement rocks, formerly known as the Older Series or Older Basalts in the south (Hughes & Turner, 1976, 1977), the Fiu Lavas in the north (Rickwood, 1957), and the Older Malaita Volcanics in the northernmost part of the island (Barron, 1993), recently have been termed the Malaita Volcanic Group (Petterson *et al.*, 1997). The Malaita Volcanic Group is distinguished in the field from an overlying, much less extensive volcanic series, previously called the Younger Series or Younger Basalts (Hughes & Turner, 1976, 1977) but now termed the Maramasike Formation (Fm.; Petterson *et al.*, 1997), by the vesicularity of the younger volcanic rocks and the intercalation of these rocks with Eocene pelagic limestones.

Samples for this study were collected in conjunction with geological mapping surveys by the Solomon Islands Ministry of Energy, Mineral and Water Resources in 1993 (see Petterson, 1995). The great bulk of the Malaita Volcanic Group exposed in the central part of the island consists of massive and pillowed lava flows very similar to those in southern Malaita, and to the Sigana Basalts (Hawkins & Barron, 1991) in northeastern Santa Isabel. The flows are aphanitic to phaneritic, aphyric to plagioclase + clinopyroxene (± olivine)-phyric basalts, and coarser-grained diabases and microgabbros [see Petterson (1995) and Babbs (1997) for detailed descriptions]. Important findings of the surveys are that all of the lavas were emplaced in a submarine environment, that interbeds of chert or mudstone are very rare, and that no limestone interbeds were found. Very few dikes were encountered, although gabbroic intrusions were found to the north, within the Fateleka Anticline (Fig. 2a). Except in disturbed sections, the basalts in central Malaita are everywhere overlain conformably by the early to middle Cretaceous Kwara'ae Mudstone Formation, consisting of siliceous, parallel-laminated radiolarian pelagic mudstones.

Our principal study area was the northern part of the Kwaio Anticline, where the thickest exposures of the Malaita Volcanic Group occur (Fig. 2a). The anticline is accessible via rivers that cut the basement and sedimentary sections in a SW–NE direction roughly perpendicular to the axis of the anticline, facilitating thickness determination of all the lithostratigraphic units. The majority of the samples we discuss here were collected from the Singgalo and Kwaimbaita rivers, where a lava section of estimated 3·5 km thickness (Petterson *et al.*, 1997) forms the core of the anticline (Fig. 2b). The other sample area we discuss is the Kwara'ae Anticline (Fig. 2a), accessible via the Kwaiafa'a River and its tributary, the Bisula, where we sampled a basement section of ~500 m thickness.

Samples were taken mainly from interior portions of pillows and massive flows, to minimize alteration. The modal mineralogy of the microgabbros and the groundmass in the aphyric and plagioclase-phyric basalts consists of almost equal proportions of unaltered plagioclase (up to 58%) and clinopyroxene (up to 45%), with minor altered olivine (5–7%) and oxides (Petterson, 1995). Plagioclase and clinopyroxene are usually in an ophitic to subophitic relationship, indicating contemporaneous crystallization, although in some sections plagioclase crystals are found included in clinopyroxene grains, possibly indicating that the plagioclase crystallized earlier. Modal abundance of mesostasis varies from 10 to 30% but usually is <20%. In the samples chosen for geochemical work, limited low-grade alteration is seen in rare amygdules containing zeolite, chlorite, and calcite, and is manifested in mesostasis and olivine, which are partially to wholly replaced by brown clay and iddingsite (Babbs, 1997). In some of the more altered samples (e.g. ML476) plagioclase is partially replaced by a mixture of clay and calcite, whereas in others (e.g. SGB24), secondary phases replace olivine completely and fill the interstices between feldspar laths. In the Kwaio Anticline, a minor but striking facies of the Malaita Volcanic Group, consisting of basalts with 'spherulitic' or 'orbicular' texture, was found as boulders in the river beds (Petterson, 1995). This facies consists of 1–6 cm fragments of ophitic gabbro and plagioclase or clinopyroxene megacrysts in basaltic to diabasic host rock.

ANALYTICAL METHODS

We collected 152 igneous rock samples, 64 of which we chose for geochemical study: 30 from the Singgalo River, 20 from the Kwaimbaita River, and 14 from the Kwaiafa'a River drainages. Samples were trimmed with a water-cooled rock saw to remove alteration rinds and split into three parts; the freshest interior portions were reserved for ^{40}Ar–^{39}Ar and isotopic analysis. Splits for

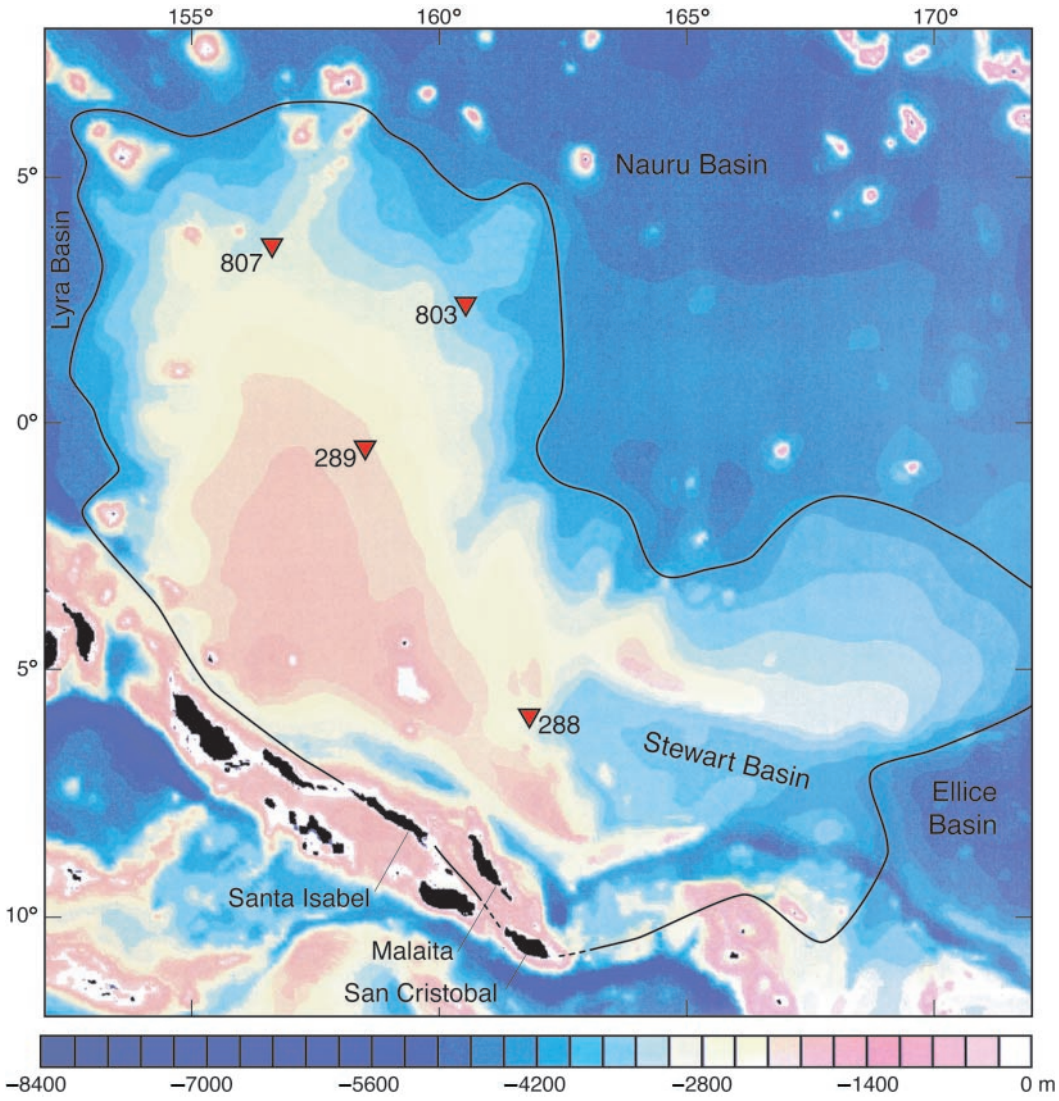

Fig. 1. Etopo 5 predicted bathymetry (in meters) of the western Pacific Basin (after Smith & Sandwell, 1996), centered on the Ontong Java Plateau. The Solomon Islands are at the plateau's southwestern margin. Also shown are the locations of ODP Sites 807 and 803, and DSDP Sites 289, where basement rocks were recovered, and 288, which recovered ~ 90 Ma and ~118 Ma ash layers but did not reach basement.

bulk-rock major and trace element analysis were chipped into pieces 0·3–0·5 cm across, cleaned ultrasonically in deionized water, and dried; chips showing macroscopic alteration significantly greater than the average were removed, and the remainder powdered in an alumina mill. Major elements and a suite of trace elements (Table 1; note that samples are listed in stratigraphic order from top to bottom of each section) were analyzed by X-ray fluorescence (XRF) spectrometry at the University of Hawaii, using the methods of Norrish & Chappell (1977). Rare earth elements and several other trace elements (Table 2) were analyzed on 0·2 g splits of the powders by inductively coupled plasma–mass spectrometry (ICP-MS) at the University of Notre Dame using the modification of Jenner *et al.*'s (1990) method proposed by McGinnis *et al.* (1997); see Jain & Neal (1996) for details. Of the elements analyzed by both XRF and ICP-MS, the agreement is generally $\leq 5\%$ for Zr and $\leq 15\%$ for Y; agreement is within 15% for Co and Nb and 20% for Cr (except for one, four, and six samples, respectively). The ICP-MS values for Rb are systematically higher than the XRF values by as much as 0·9 ppm; however, the analytical uncertainty of the XRF measurements is relatively large as Rb contents are generally near the XRF detection limit.

Splits of eight whole-rock samples were prepared at Oregon State University for ^{40}Ar–^{39}Ar incremental-heating age determinations. Small cores (~0·7 g) cut from the freshest portions of samples were loaded in evacuated quartz vials and irradiated for 6 h at 1 MW power at

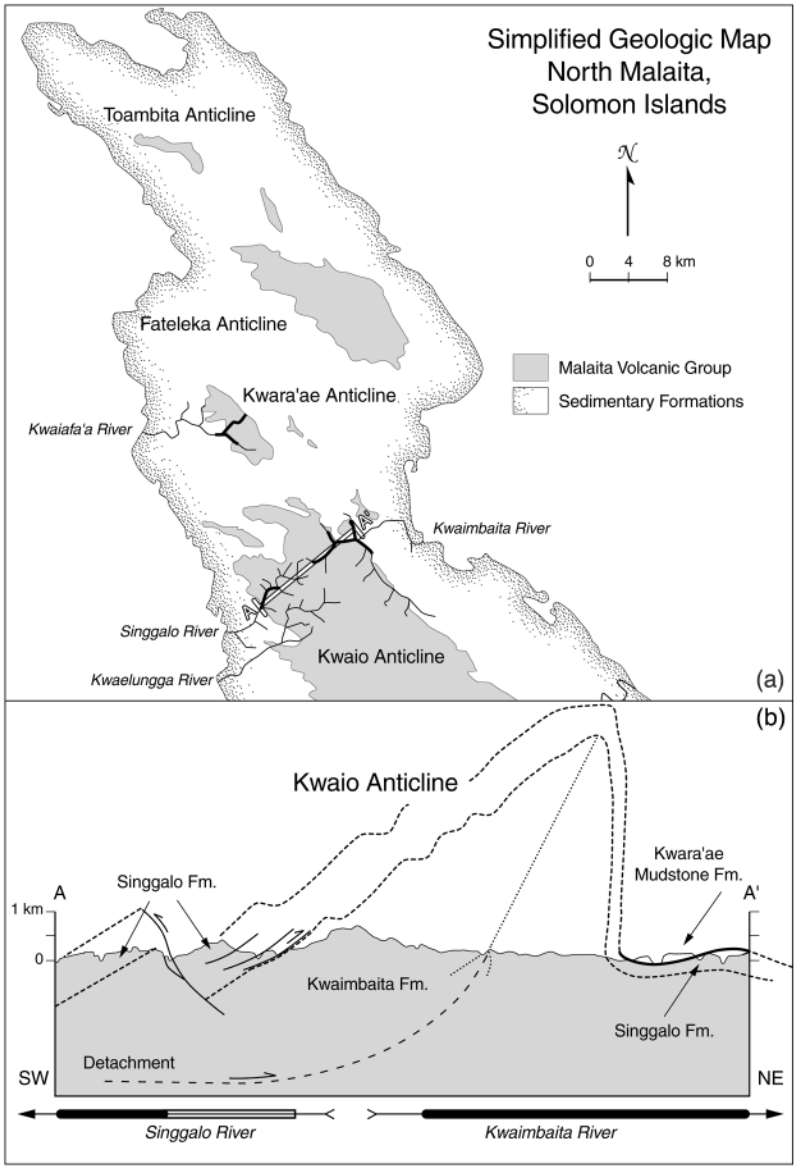

Fig. 2. (a) Simplified geologic map of the northern half of Malaita showing the anticlines where exposures of the Malaita Volcanic Group are found (after Petterson, 1995). The rivers traversed are shown with heavier-outlined portions indicating sampling coverage. The line A–A′ represents the projection line for the cross-section in (b). (b) Basement structure along the Singgalo and Kwaimbaita rivers (after Petterson *et al.*, 1997); the boundary between the two chemical groups of lavas we term the Singgalo Fm. and Kwaimbaita Fm. (see text) is determined from isotopic and chemical data. The arrows at the bottom indicate flow directions of the Singgalo and Kwaimbaita rivers, and the filled bars represent our sampling coverage. The open bar along the upper Singgalo River shows the extent of sampling conducted by T. Babbs and A. Saunders (Babbs, 1997).

the Oregon State University TRIGA reactor. Biotite standard FCT-3 (27·55 ± 0·12 Ma, equivalent to 513·9 Ma for hornblende Mmhb-1; Lanphere *et al.*, 1990) was used to monitor the neutron fluence. The isotopic composition of Ar was determined for each of 4–6 temperature steps using an AEI MS-10S mass spectrometer [see Duncan *et al.* (1997) for experimental details]. Table 3 includes plateau ages (the weighted mean of concordant, adjacent step ages), isochron ages (determined from the linear regression of step compositions), and integrated or total fusion ages (calculated by adding all step compositions together).

Sample preparation and analysis for Sr, Nd, and Pb isotopes were performed at the University of Hawaii [for methods, see Peng & Mahoney (1995) and Tejada *et al.* (1996)]. Isotope-dilution abundance data for Sr, Rb, Nd,

Table 1: X-ray fluorescence major and trace element data for central Malaita basement rocks

Sample	SiO_2	TiO_2	Al_2O_3	Fe_2O_3*	MnO	MgO	CaO	Na_2O	K_2O	P_2O_5	SUM	LOI	Rb	Nb	Sr	Zr	V	Y	Sc	Zn	Cu	Co	Mn	Ni	Cr
Kwaio Anticline																									
Singgalo River																									
SG1	50·38	1·65	13·54	14·01	0·19	7·30	11·64	2·32	0·15	0·14	101·32	0·30	1·8	4·4	136	81	392	29	41	93	124			61	
SG2	49·65	1·59	14·15	13·68	0·18	7·69	11·25	2·30	0·16	0·14	100·79	0·71	1·9	4·3	141	78	372	25	38	87	99			85	
SG3	49·75	1·52	14·31	13·82	0·18	7·59	11·14	2·30	0·17	0·15	100·93	0·67	1·8	4·9	144	88	329	28	34	90	97			74	
SG4	49·98	1·62	14·22	13·85	0·19	6·99	11·34	2·38	0·11	0·15	100·83	0·51	<1·5	5·4	143	93	395	28	41	99	96			62	
SG5	49·73	1·57	14·70	12·54	0·18	7·44	11·29	2·43	0·19	0·15	100·22	0·89	1·9	5·2	145	91	395	28	44	96	94			71	
SG6	49·50	1·57	14·36	12·98	0·19	7·01	12·52	2·42	0·16	0·14	100·85	1·56	<1·5	4·5	146	80	384	28	39	89	103			86	
SG7	50·18	1·67	14·19	13·83	0·19	6·86	11·28	2·48	0·14	0·16	100·98	0·42	<1·5	5·5	145	98	376	31	42	102	92			70	
SGB1	49·59	1·68	13·92	13·92	0·18	7·04	10·86	2·44	0·18	0·15	99·96	0·74	1·6	5·5	139	92	383	29	43	96	96			67	
SGB2	49·96	1·60	14·47	13·06	0·19	6·88	11·23	2·52	0·20	0·16	100·27	1·24	1·9	5·8	145	94	397	30	49	104	93			73	
SGB6	50·07	1·68	14·33	13·29	0·19	7·02	11·11	2·25	0·15	0·14	100·23	0·28	<1·5	5·6	146	97	390	30	42	118	109	52	1440	79	123
SGB7	49·83	1·64	14·11	13·93	0·19	7·04	11·41	2·00	0·16	0·13	100·44	0·71	2·1	4·7	146	90	342	30	36	97	107	47	1290	73	107
SGB8	50·39	1·77	14·33	13·63	0·18	6·87	10·93	2·26	0·16	0·14	100·66	0·75	<1·5	5·6	148	99	367	31	36	110	116	50	1230	71	90
SGB3	49·45	1·62	13·98	14·24	0·20	6·34	11·52	2·35	0·11	0·15	99·96	0·52	<1·5	5·5	146	96	353	30	39	102	94			71	
SGB4	49·62	1·62	14·05	14·33	0·20	6·72	11·46	2·40	0·13	0·16	100·69	0·71	<1·5	5·8	145	95	351	30	38	100	92			72	
SGB5	49·89	1·40	14·48	13·71	0·18	6·95	11·59	1·82	0·16	0·13	100·31	1·02	1·7	5·3	151	93	327	29	31	103	113	48	1160	76	80
SGB9	49·39	1·49	14·51	13·14	0·20	7·44	11·88	2·09	0·14	0·12	100·40	0·24	2·0	4·2	152	78	308	26	33	86	115	46	1380	87	154
SGB12	48·82	1·53	15·13	12·91	0·21	7·14	11·31	2·15	0·14	0·15	99·49	1·08	<1·5	5·6	150	99	427	31	50	111	109	54	1640	77	153
SGB10	49·92	1·35	14·01	14·37	0·20	6·81	10·95	2·21	0·17	0·14	100·13	0·46	2·6	6·0	141	92	360	30	38	106	102	47	1380	64	100
SGB11	49·11	1·39	14·24	14·26	0·21	7·15	11·64	2·19	0·08	0·15	100·42	0·17	<1·5	5·2	147	96	367	31	38	105	108	50	1520	78	118
SGB13	50·00	1·48	14·17	13·73	0·20	6·86	11·14	2·30	0·16	0·15	100·19	0·45	<1·5	5·8	148	100	349	32	38	104	105	49	1430	72	106
SGB14	49·70	1·50	14·09	14·26	0·20	6·94	11·23	2·21	0·18	0·14	100·45	0·68	2·2	5·5	148	96	319	31	32	129	110	49	1370	74	91
SGB16	49·05	1·37	14·19	14·02	0·19	7·34	11·45	2·16	0·11	0·14	100·02	1·04	<1·5	5·0	147	94	320	30	31	95	115	50	1240	85	95
SGB15	49·39	1·13	14·46	13·04	0·19	7·35	12·25	2·05	0·12	0·11	100·09	0·78	<1·5	4·3	143	76	307	25	32	88	128	48	1360	86	110
SGB17	49·48	1·18	14·11	13·50	0·21	7·14	11·99	2·02	0·14	0·12	99·89	0·50	1·7	4·5	141	83	326	27	32	101	129	49	1430	76	84
SGB18	49·01	0·88	14·72	12·72	0·18	7·42	13·03	1·81	0·10	0·10	99·97	0·51	<1·5	3·3	121	66	300	23	41	87	142	53	1360	99	198
SGB22	48·93	0·98	14·65	12·86	0·19	7·41	12·95	1·84	0·09	0·10	100·00	0·35	<1·5	3·1	124	67	318	23	42	91	145	53	1490	99	184
SGB23	49·00	1·05	14·37	13·10	0·19	7·54	12·77	1·83	0·10	0·10	100·05	0·63	<1·5	3·8	123	69	314	24	37	90	150	54	1320	96	159
SGB24	48·99	0·93	14·79	12·19	0·18	8·19	11·77	2·84	0·31	0·08	100·27	2·70	2·6	2·4	219	48	250	19	35	64	139	50	1140	101	189
SGB25	48·96	0·93	14·78	12·56	0·21	7·86	13·16	1·51	0·05	0·10	100·12	0·49	<1·5	3·6	122	65	320	22	45	92	141	52	1660	105	213

Table 1: continued

Sample	SiO_2	TiO_2	Al_2O_3	Fe_2O_3*	MnO	MgO	CaO	Na_2O	K_2O	P_2O_5	SUM	LOI	Rb	Nb	Sr	Zr	V	Y	Sc	Zn	Cu	Co	Mn	Ni	Cr
Kwaimbaita River																									
ML407	49·67	1·35	13·64	13·47	0·19	7·45	11·38	3·08	0·26	0·13	100·62	2·14	2·6	3·8	291	71	295	25	40	57	229			62	
ML476	47·88	2·07	13·21	18·49	0·25	5·83	9·61	3·08	0·09	0·17	100·68	3·62	<1·5	5·5	129	101	407	33	31	111	174			35	
ML475	49·68	0·73	14·00	9·84	0·16	9·99	14·52	1·48	0·08	0·06	100·54	1·91	<1·5	1·6	128	28	217	13	40	47	128			133	
ML474	48·60	1·33	14·75	13·03	0·22	7·10	12·63	2·13	0·05	0·13	99·97	1·12	<1·5	4·2	155	73	324	25	45	89	137			104	
ML436	49·06	1·27	14·55	12·41	0·22	7·82	12·67	2·18	0·14	0·12	100·44	0·94	<1·5	3·8	139	71	325	24	47	86	130			110	
ML434	49·28	1·25	14·40	12·41	0·22	8·00	12·57	2·14	0·21	0·13	100·61	1·14	<1·5	3·9	138	69	316	23	45	81	124			103	
ML432	49·30	1·24	14·69	12·35	0·24	8·05	12·66	1·91	0·12	0·12	100·68	2·51	1·6	3·2	180	64	314	22	37	68	143			99	
ML431	49·05	1·30	14·60	12·63	0·20	7·80	12·87	2·00	0·06	0·12	100·63	0·71	<1·5	3·5	121	66	305	23	42	84	137			97	
ML423	48·96	1·22	14·67	12·86	0·21	7·40	13·22	2·05	0·05	0·12	100·76	0·50	<1·5	3·4	122	64	296	22	41	77	133			97	
ML422	49·24	1·22	14·75	11·93	0·26	7·95	12·87	2·14	0·06	0·12	100·54	0·45	<1·5	3·7	154	69	328	24	45	90	143			95	
ML451	48·96	1·24	14·39	13·06	0·19	8·93	11·96	1·87	0·10	0·12	100·82	1·55	<1·5	3·2	129	62	316	22	29	78	150			125	
ML450	49·50	1·60	14·28	13·37	0·19	7·42	11·66	2·28	0·14	0·14	100·58	0·94	2·0	4·5	133	81	371	27	37	82	109			74	
ML449	50·09	1·69	14·80	13·04	0·19	7·25	10·42	2·45	0·19	0·16	100·28	0·95	1·7	5·7	146	95	412	30	48	101	100			76	
ML421	49·17	1·76	14·18	13·94	0·19	7·66	11·06	2·34	0·07	0·16	100·53	0·84	<1·5	5·7	146	96	405	29	42	105	98			67	
ML437	49·33	1·59	14·39	13·62	0·22	7·78	11·25	2·27	0·17	0·14	100·76	0·93	2·0	4·8	135	83	367	27	38	90	112			75	
ML438	49·76	1·59	13·87	14·23	0·19	7·20	10·75	2·33	0·18	0·15	100·25	0·80	2·1	5·0	142	92	374	29	36	118	104			54	
ML439	49·00	1·70	14·49	13·76	0·25	7·21	11·50	2·46	0·09	0·16	100·62	0·38	<1·5	5·7	149	100	409	31	49	109	95			62	
ML440	49·60	1·36	14·09	13·56	0·18	7·65	11·68	2·26	0·15	0·14	100·67	0·72	2·0	4·6	131	80	321	26	33	81	111			80	
ML448	50·31	1·61	14·41	12·92	0·22	7·89	10·51	2·44	0·18	0·16	100·65	0·99	<1·5	5·4	148	94	410	33	43	119	97			74	
ML468	48·86	1·71	14·32	14·58	0·20	7·56	10·85	2·26	0·08	0·16	100·58	1·07	<1·5	5·8	148	95	401	29	45	109	96			60	
Kwara'ae Anticline																									
Kwaiafa'a River																									
KF-1	50·13	1·28	14·35	12·23	0·19	8·09	10·90	2·94	0·23	0·08	100·41	1·94	3·0	3·5	127	59	293	20	31	70	117	55	1213	96	155
KF-4	50·47	1·72	13·77	14·22	0·21	6·60	11·03	2·03	0·13	0·14	100·31	0·50	2·2	5·7	152	101	441	31	34	102	115	41	1448	40	29
KF-9	49·79	1·56	14·06	14·13	0·21	6·39	11·50	1·98	0·15	0·14	99·91	0·49	2·1	5·5	144	97	334	30	37	102	104	49	1470	71	116
KF-13	48·63	1·59	14·55	14·35	0·21	6·80	11·88	1·65	0·04	0·14	99·83	0·42	<1·5	5·8	147	102	352	32	36	107	111	53	1578	80	115
KF-14	49·73	1·56	14·20	13·81	0·19	6·86	11·44	2·04	0·05	0·13	100·01	0·30	<1·5	5·5	146	96	343	31	35	106	105	48	1346	69	111
KF-19	49·48	1·62	14·11	14·02	0·20	7·02	11·18	1·94	0·08	0·12	99·77	0·41	<1·5	4·6	145	88	379	27	38	103	115	49	1474	69	116
KF-24	48·81	1·63	14·40	13·50	0·22	7·61	11·28	2·03	0·06	0·14	99·68	0·80	<1·5	5·6	218	96	389	28	43	105	107	56	1703	73	126

Sample	SiO_2	TiO_2	Al_2O_3	Fe_2O_3*	MnO	MgO	CaO	Na_2O	K_2O	P_2O_5	SUM	LOI	Rb	Nb	Sr	Zr	V	Y	Sc	Zn	Cu	Co	Mn	Ni	Cr
KF-30	49·56	1·52	13·95	13·81	0·28	7·10	11·12	1·83	0·12	0·12	99·41	0·57	<1·5	4·8	135	88	369	27	41	101	115	50	2326	66	119
KF-31	49·74	1·57	14·20	13·93	0·20	6·75	10·95	2·04	0·14	0·13	99·65	0·74	1·8	5·1	146	93	334	30	33	94	111	45	1325	66	99
KF-32	49·65	1·27	15·87	12·06	0·18	7·04	12·25	1·85	0·09	0·11	100·37	0·86	<1·5	4·0	151	74	265	24	33	72	120	45	1274	91	154
KF-36	49·60	1·62	14·08	13·78	0·20	6·74	11·45	1·98	0·14	0·12	99·71	0·90	1·7	5·0	143	92	343	30	36	121	108	52	1463	75	120
KF-43	49·84	1·66	14·25	14·06	0·20	6·69	10·99	2·08	0·12	0·14	100·03	0·55	<1·5	5·3	145	98	337	30	35	106	105	47	1397	59	95
KF-49	49·25	1·70	14·54	12·22	0·21	6·81	12·57	1·93	0·15	0·13	99·51	2·23	1·5	5·5	148	91	401	32	43	90	111	52	1525	63	108
KF-53	49·89	1·56	14·70	13·19	0·19	6·73	11·20	2·06	0·11	0·13	99·76	0·41	<1·5	5·4	139	91	395	30	49	106	113	53	1537	81	170
University of Hawaii analyses of standards																									
BCR-1	54·39	2·36	13·60	13·65	0·18	3·58	6·98	3·52	1·71	0·39	100·35		47·4	12	329	195	410	37	31	126	18	36	1331	12	5
SD (n = 6)	0·08	0·05	0·02	0·05	0·00	0·02	0·03	0·04	0·01	0·00			0·1	0·2	1	1	3	0	1	1	1	2	10	1	3
BHVO-1	49·47	2·85	13·69	12·41	0·17	7·24	11·36	2·43	0·53	0·29	100·42		8·8	18·4	387	177	317	27	32	100	133	45	1280	115	284
SD (n = 6)	0·09	0·06	0·04	0·02	0·00	0·01	0·02	0·03	0·01	0·00			0·1	0·2	1	0	3	0	1	2	1	2	2	2	0
Recommended values (Govindaraju, 1994)																									
BCR-1	54·44	2·25	13·72	13·54	0·18	3·50	6·99	3·29	1·70	0·36	99·98		47·2	14	330	190	407	38	33	130	19	37	1371	13	16
BHVO-1	49·59	2·69	13·70	12·27	0·17	7·18	11·32	2·24	0·52	0·27	99·95		9·5	19	390	179	317	28	32	105	136	45	1262	121	289

Major element oxides are in weight percent; trace elements are in ppm. LOI, weight loss on ignition to 900°C for at least 10 h. Fe_2O_3*, all Fe as Fe_2O_3. Estimated relative uncertainties on major and minor elements are 1%, except for SiO_2, which is 0·5%. For trace elements, estimated average overall uncertainties based on measurements of standards AGV-1, BCR-1, BHVO-1, and W-1 are (in ppm): 0·3 for Rb, 0·2 for Nb, 1·0 for Sr, 1·0 for Zr, 3·5 for V, 0·3 for Y, 1·4 for Sc, 2·5 for Cr, 2·1 for Zn, 1·5 for Ni, 2·0 for Cu, 2·1 for Co, and 10 for Mn. An indication of accuracy is given by measured values of standards BCR-1 and BHVO-1 and recommended working values (Govindaraju, 1994). The dashed lines define the boundary between the two chemical groups of lavas along the Singgalo and Kwaimbaita river sections.

Table 2: ICP-MS data for central Malaita basement rocks

	Li	Cs	Rb	Ba	Th	U	Nb	Ta	La	Ce	Pr	Sr	Nd	Zr	Hf	Sm	Eu	Gd	Tb	Dy	Y	Ho	Er	Tm	Yb	Lu	Mo	Ga	Co	Cr
Kwaio Anticline																														
Singgalo River																														
SG1	6·03	0·01	2·4	28	0·61	0·13	4·9	0·35	4·75	12·6	1·98	138	9·81	81	2·50	3·23	1·13	4·14	0·73	4·56	25	1·00	2·90	0·41	2·83	0·43	0·59	17	51	56
SG2	10·41	0·01	2·4	30	0·57	0·13	4·9	0·34	4·62	12·5	1·83	145	9·48	79	2·40	3·00	1·17	3·79	0·68	4·21	23	0·93	2·58	0·36	2·51	0·38	0·49	16	46	81
SG3	8·17	0·02	2·5	33	0·61	0·14	5·6	0·37	5·15	14·0	2·10	146	10·6	89	2·88	3·22	1·10	4·10	0·73	4·45	26	1·00	2·93	0·41	2·81	0·42	0·53	22	61	114
SG4	7·02	0·03	0·9	31	0·44	0·16	5·6	0·39	5·50	14·4	2·32	144	11·6	94	2·79	3·43	1·21	4·44	0·79	4·91	28	1·08	3·12	0·44	3·05	0·46	0·66	19	51	74
SG5	5·60	0·03	2·7	38	0·52	0·15	5·4	0·37	5·42	14·3	2·17	152	10·9	91	2·64	3·43	1·27	4·37	0·75	4·91	25	0·99	2·79	0·42	3·12	0·49	0·36	15	39	62
SG6	6·56	0·02	1·4	31	0·45	0·13	5·1	0·36	5·33	13·8	1·93	148	9·80	83	2·61	3·12	1·09	4·02	0·72	4·57	26	0·98	2·84	0·40	2·75	0·42	0·49	17	48	95
SG7	5·97	0·01	1·0	33	0·60	0·16	5·9	0·40	5·90	15·9	2·27	148	11·6	96	2·83	3·69	1·23	4·70	0·84	5·14	29	1·11	3·10	0·44	3·00	0·45	1·13	19	50	84
SGB1	6·46	0·01	2·4	37	0·59	0·15	5·9	0·40	5·63	14·8	2·15	148	11·3	93	2·97	3·41	1·20	4·38	0·75	4·74	28	1·08	3·06	0·44	3·02	0·46	0·75	19	49	92
SGB2	7·35	0·02	2·8	44	0·54	0·17	6·0	0·41	5·57	14·8	2·26	149	11·0	94	3·03	3·45	1·19	4·25	0·78	4·79	28	1·03	3·00	0·42	2·93	0·45	0·64	19	49	95
SGB6	6·23	0·03	1·6	33	0·49	0·16	5·8	0·38	5·59	15·4	2·21	152	11·2	101	2·89	3·60	1·22	4·56	0·79	5·04	27	1·07	2·98	0·42	2·86	0·43	0·59	18	50	89
SGB7	5·40	0·02	2·2	36	0·56	0·14	5·3	0·36	5·71	15·0	2·46	141	12·5	93	2·75	3·54	1·28	4·44	0·85	5·17	29	1·07	3·16	0·47	3·10	0·47	0·61	18	48	91
SGB8	6·15	0·02	1·5	37	0·66	0·15	5·8	0·38	5·45	15·3	2·19	146	11·2	99	2·85	3·57	1·23	4·51	0·82	5·08	28	1·09	3·05	0·43	2·91	0·44	1·00	19	47	89
SGB3	6·81	0·02	1·1	30	0·65	0·17	5·9	0·41	5·75	15·3	2·40	159	12·1	95	2·96	3·60	1·25	4·51	0·81	4·95	30	1·07	3·06	0·44	3·02	0·46	0·60	18	49	89
SGB4	6·18	0·02	1·5	30	0·56	0·19	5·7	0·39	5·64	15·0	2·24	146	11·5	94	2·94	3·52	1·25	4·42	0·81	5·03	30	1·07	2·98	0·42	2·91	0·44	0·66	18	48	84
SGB5	6·95	0·02	1·8	29	0·53	0·15	5·7	0·38	5·14	14·4	2·03	141	10·8	95	2·75	3·34	1·15	4·13	0·78	4·80	29	1·02	2·92	0·41	2·84	0·43	0·70	18	47	84
SGB9	4·86	0·01	2·0	32	0·56	0·13	5·1	0·33	6·03	16·0	2·44	144	11·9	77	2·56	3·08	1·08	4·67	0·74	4·38	25	0·94	2·72	0·38	2·64	0·40	0·54	18	48	138
SGB12	6·38	0·01	0·8	33	0·60	0·16	6·4	0·41	5·61	15·8	2·28	162	11·9	99	3·11	3·62	1·32	4·62	0·83	5·29	30	1·12	3·17	0·44	3·02	0·45	0·45	19	49	92
SGB10	5·78	0·02	2·2	36	0·57	0·15	5·8	0·38	5·70	15·7	2·27	142	11·6	94	2·87	3·52	1·24	4·55	0·82	5·12	29	1·08	3·09	0·43	2·98	0·45	0·86	18	47	83
SGB11	5·37	0·02	0·5	25	0·64	0·15	5·9	0·38	5·71	15·5	2·22	150	11·4	100	2·84	3·54	1·21	4·53	0·82	5·05	30	1·08	3·10	0·43	2·97	0·45	2·26	18	49	83
SGB13	6·52	0·01	1·5	37	0·52	0·15	6·2	0·40	6·26	16·8	2·38	155	12·2	101	2·93	3·89	1·31	4·83	0·86	5·34	30	1·14	3·22	0·45	3·05	0·46	0·63	18	49	81
SGB14	6·51	0·02	2·2	36	0·61	0·16	5·9	0·39	5·64	15·4	2·16	146	11·0	99	2·91	3·54	1·21	4·51	0·79	4·99	29	1·08	3·01	0·42	2·89	0·44	0·86	19	49	79
SGB16	5·50	0·02	1·0	31	0·62	0·14	5·7	0·35	5·53	15·1	2·30	140	11·6	97	2·70	3·33	1·23	4·51	0·80	4·77	28	0·99	2·80	0·42	2·93	0·44	0·57	18	50	100
SGB15	6·38	0·01	1·4	17	0·39	0·11	4·5	0·30	4·38	12·1	1·72	136	8·82	78	2·20	2·88	1·02	3·72	0·69	4·11	24	0·92	2·49	0·35	2·33	0·35	0·46	17	51	103
SGB17	6·07	0·02	1·9	20	0·50	0·13	5·0	0·32	4·69	12·9	1·86	134	9·69	83	2·47	3·05	1·04	3·81	0·70	4·37	27	0·96	2·64	0·37	2·51	0·38	0·53	17	50	88
SGB18	4·91	0·01	1·4	13	0·35	0·08	3·7	0·23	3·30	9·75	1·41	125	7·64	69	2·00	2·48	0·88	3·20	0·60	3·76	21	0·83	2·29	0·32	2·16	0·32	0·37	16	50	133
SGB22	4·17	0·01	1·0	13	0·34	0·09	3·9	0·26	3·41	9·77	1·48	127	7·76	68	2·08	2·55	0·92	3·34	0·62	3·86	23	0·85	2·34	0·33	2·21	0·33	0·82	16	53	133
SGB23	4·71		1·2	14	0·34	0·10	4·1	0·27	3·56	10·2	1·50	123	7·97	71	2·06	2·64	0·93	3·44	0·64	4·01	21	0·89	2·49	0·35	2·35	0·35	0·74	16	52	123
SGB24	7·72	0·02	2·5	41	0·28	0·07	3·2	0·21	3·15	9·29	1·34	211	7·07	52	1·42	2·39	0·89	3·06	0·57	3·51	16	0·74	2·10	0·30	2·05	0·31	0·27	16	47	127
SGB25	4·60	0·01	0·46	12	0·34	0·09	3·7	0·25	3·52	9·58	1·51	126	8·12	68	1·98	2·55	0·91	3·46	0·59	3·67	21	0·81	2·23	0·34	2·37	0·36	0·18	16	53	139

	Li	Cs	Rb	Ba	Th	U	Nb	Ta	La	Ce	Pr	Sr	Nd	Zr	Hf	Sm	Eu	Gd	Tb	Dy	Y	Ho	Er	Tm	Yb	Lu	Mo	Ga	Co	Cr
Kwaimbaita River																														
ML407	4·99	0·01	2·9	23	0·33	0·09	5·0	0·25	3·86	10·6	1·70	288	8·75	83	2·63	2·97	0·94	3·54	0·68	4·22	23	0·92	2·57	0·36	2·47	0·37	0·36	17	50	61
ML476	5·20	0·02	1·4	13	0·56	0·13	6·5	0·40	5·44	16·4	2·26	129	11·9	102	2·95	3·73	1·28	4·71	0·86	5·25	32	1·10	3·19	0·44	3·01	0·45	0·39	22	52	101
ML475	3·51	0·01	0·9	11	0·10	0·04	2·7	0·16	1·61	4·80	0·72	135	3·78	30	1·09	1·30	0·51	1·74	0·32	2·05	10	0·43	1·26	0·17	1·16	0·17	0·18	13	39	446
ML474	7·00	0·01	0·3	12	0·36	0·12	4·7	0·27	3·77	10·4	1·58	160	8·49	74	2·80	2·69	1·02	3·44	0·64	4·21	26	0·87	2·58	0·38	2·59	0·42	0·15	17	46	122
ML436	8·59	0·01	0·8	20	0·31	0·09	4·0	0·25	3·48	10·6	1·50	140	8·04	73	1·98	2·62	0·89	3·29	0·59	3·65	22	0·76	2·16	0·31	2·19	0·34	0·21	17	51	155
ML434	9·76		1·3	28	0·28	0·09	3·8	0·23	3·36	10·1	1·44	147	7·64	69	2·23	2·49	0·85	3·09	0·56	3·40	23	0·70	2·06	0·29	1·94	0·29	0·27	16	47	143
ML432	8·79	0·01	1·6	30	0·31	0·09	3·8	0·24	3·00	9·10	1·34	169	7·30	65	2·00	2·43	0·89	3·04	0·57	3·45	19	0·74	2·09	0·29	1·98	0·30	0·30	17	54	130
ML431	4·78	0·01	0·6	15	0·34	0·08	3·6	0·24	3·49	10·3	1·43	121	7·69	67	1·91	2·40	0·90	3·14	0·58	3·64	22	0·76	2·20	0·31	2·10	0·32	0·85	16	51	128
ML423	4·17		0·5	12	0·27	0·08	3·1	0·19	3·44	9·84	1·51	130	7·93	66	2·12	2·53	0·89	3·31	0·60	3·72	16	0·82	2·38	0·33	2·29	0·35	0·75	19	51	128
ML422	4·22		0·7	14	0·25	0·08	3·4	0·22	3·30	9·60	1·46	157	8·09	64	2·29	2·63	0·96	3·42	0·61	3·81	19	0·86	2·43	0·34	2·34	0·35	0·52	13	42	100
ML451	20·4	0·01	0·8	16	0·32	0·07	2·9	0·20	2·95	8·87	1·25	115	6·85	56	1·63	2·25	0·82	2·86	0·55	3·31	21	0·69	1·98	0·28	1·88	0·28	0·33	16	49	134
ML450	5·20		2·5	31	0·55	0·13	5·2	0·34	5·18	13·6	2·13	140	10·4	82	2·50	3·21	1·22	4·21	0·74	4·56	24	0·95	2·76	0·39	2·59	0·44	0·49	19	46	86
ML449	8·05	0·01	2·1	39	0·44	0·16	6·1	0·39	5·72	16·1	2·19	146	11·1	99	2·88	3·45	1·20	4·32	0·76	4·62	29	0·98	2·75	0·38	2·62	0·39	0·45	21	50	100
ML421	5·96	0·01	0·4	21	0·47	0·16	6·2	0·40	5·46	14·9	2·21	152	11·0	99	2·94	3·56	1·22	4·28	0·76	4·81	27	1·05	2·96	0·42	2·84	0·43	0·46	19	49	91
ML437	4·55	0·02	2·0	42	0·58	0·11	4·7	0·29	4·80	13·6	1·83	124	9·65	86	2·17	3·03	1·06	3·89	0·69	4·32	27	0·91	2·60	0·36	2·48	0·37	1·17	19	50	110
ML438	6·83	0·02	2·0	31	0·58	0·14	5·7	0·35	5·33	15·0	2·08	135	10·7	94	2·58	3·33	1·15	4·19	0·73	4·47	27	0·95	2·69	0·37	2·54	0·38	0·50	19	50	74
ML439	8·82	0·02	0·5	19	0·58	0·16	6·2	0·40	5·76	16·5	2·24	153	11·8	99	2·94	3·55	1·21	4·39	0·77	4·74	28	1·01	2·85	0·40	2·72	0·41	0·59	19	48	65
ML440	10·11	0·02	2·0	27	0·45	0·13	4·9	0·31	4·61	13·1	1·78	130	9·36	79	2·35	2·85	1·02	3·69	0·64	4·01	26	0·85	2·43	0·34	2·30	0·34	1·04	18	48	108
ML448	6·32	0·01	1·8	33	0·44	0·11	6·0	0·37	5·61	16·2	2·23	143	11·4	76	2·25	3·43	1·17	4·40	0·77	4·73	31	1·01	2·68	0·38	2·56	0·38	0·54	20	51	95
ML468	6·88	0·02	0·6	41	0·67	0·16	6·2	0·42	4·98	14·5	2·02	156	10·5	98	3·02	3·31	1·16	4·03	0·72	4·51	28	0·94	2·65	0·37	2·55	0·38	0·75	20	46	71

Table 2: continued

	Li	Cs	Rb	Ba	Th	U	Nb	Ta	La	Ce	Pr	Sr	Nd	Zr	Hf	Sm	Eu	Gd	Tb	Dy	Y	Ho	Er	Tm	Yb	Lu	Mo	Ga	Co	Cr
Kwara'ae Anticline																														
Kwaiafa'a River																														
KF1	6·48	0·11	3·3	133	0·27	0·08	3·5	0·24	4·06	11·0	1·64	116	8·14	60	1·73	2·55	1·08	3·14	0·55	3·49	18	0·71	2·11	0·29	1·94	0·29	0·17	18	55	155
KF4	5·27	0·04	2·3	28	0·56	0·15	6·0	0·39	6·38	19·6	2·94	137	14·0	106	3·02	4·25	1·65	5·17	0·90	5·84	30	1·18	3·49	0·50	3·30	0·47	0·47	22	51	34
KF9	6·67	0·02	2·5	32	0·52	0·15	5·6	0·38	6·11	18·2	2·72	142	13·4	100	2·80	3·97	1·54	4·84	0·87	5·57	29	1·11	3·29	0·48	3·15	0·45	0·80	22	55	113
KF13	6·34	0·01	0·6	16	0·68	0·19	6·1	0·39	6·27	19·1	2·84	145	14·1	125	3·45	4·29	1·59	5·12	0·92	6·04	32	1·23	3·69	0·53	3·51	0·51	0·31	22	56	101
KF14	5·73	0·01	0·8	24	0·53	0·15	5·5	0·37	5·96	18·0	2·63	145	13·0	98	2·78	3·92	1·48	4·79	0·86	5·46	28	1·12	3·21	0·46	3·08	0·44	0·96	21	54	100
KF19	5·51	0·01	0·9	24	0·45	0·15	5·2	0·34	4·97	15·4	2·34	141	11·7	93	2·65	3·54	1·40	4·37	0·77	5·00	24	1·01	2·98	0·41	2·83	0·40	2·76	21	53	99
KF24	7·63	0·04	0·7	50	0·56	0·17	5·8	0·37	5·76	17·7	2·69	207	13·0	106	2·99	3·87	1·54	4·91	0·85	5·56	28	1·12	3·23	0·46	3·12	0·44	0·42	21	60	94
KF30	7·26	0·01	2·0	26	0·64	0·16	5·7	0·37	5·83	17·9	2·70	134	13·4	106	2·98	4·02	1·56	4·93	0·86	5·63	29	1·14	3·38	0·47	3·38	0·47	1·49	21	55	97
KF31	5·31	0·01	1·9	30	0·53	0·15	5·5	0·36	6·06	18·1	2·70	134	13·2	98	2·82	4·09	1·52	4·90	0·84	5·51	29	1·13	3·31	0·46	3·07	0·45	0·61	21	55	99
KF32	4·84	0·01	1·6	22	0·38	0·11	4·1	0·27	4·43	13·4	2·03	138	9·77	73	2·10	2·98	1·18	3·66	0·65	4·24	22	0·86	2·55	0·36	2·42	0·34	0·31	20	55	168
KF36	5·39	0·01	2·5	28	0·53	0·15	5·4	0·36	5·76	17·0	2·52	140	12·8	94	2·70	3·90	1·49	4·69	0·83	5·41	28	1·12	3·26	0·47	3·06	0·44	0·58	21	54	105
KF43	5·77	0·01	1·6	29	0·57	0·16	5·9	0·38	6·07	18·2	2·72	143	13·5	104	2·98	3·99	1·54	4·83	0·88	5·59	28	1·15	3·36	0·48	3·22	0·46	0·97	21	52	79
KF49	7·61	0·02	2·0	37	0·53	0·15	5·5	0·36	6·21	18·5	2·75	145	13·4	96	2·76	4·06	1·55	5·06	0·90	6·03	31	1·20	3·60	0·52	3·39	0·48	0·32	21	55	91
KF53	7·07	0·02	2·0	57	0·51	0·14	5·4	0·35	5·79	17·3	2·59	142	12·9	94	2·78	3·96	1·49	4·90	0·86	5·60	29	1·14	3·39	0·48	3·14	0·46	0·44	21	56	158
University of Notre Dame analyses of standard reference materials																														
BHVO-1	4·52	0·11	9·4	135	1·20	0·41	19	1·23	15·6	39·8	5·52	409	24·7	170	4·48	6·13	2·11	6·19	0·95	5·37	24	0·96	2·53	0·32	2·07	0·26	1·01	22	47	306
2σ (n = 52)	0·38	0·04	0·4	2	0·07	0·04	2·0	0·12	0·25	1·34	0·18	14	0·48	6	0·25	0·17	0·08	0·38	0·06	0·11	1	0·06	0·12	0·04	0·08	0·04	0·21	1	2	29
Recommended values (Govindaraju, 1994)																														
BHVO-1	4·60	0·13	11	139	1·08	0·42	19	1·23	15·8	39	5·7	403	25·2	179	4·38	6·2	2·06	6·4	0·96	5·2	28	0·99	2·4	0·33	2·02	0·29	1·02		45	289

All abundances are in ppm. Accuracy is illustrated by the published and measured values of BHVO-1. Estimated uncertainties from 52 analyses of BHVO-1 standard are <10% for most elements except for Ba, La, Nd, Dy (<5%), Th, Nb, Gd, Tb, Ho (<15%), U, Ta, Cr (19%), Tm (27%), and Lu (30%). Recommended values are from Govindaraju (1994). Errors on the means for the BHVO-1 data are 2 SD. The dashed lines define the boundary between the two chemical groups of lavas along the Singgalo and Kwaimbaita river sections.

Table 3: ^{40}Ar–^{39}Ar incremental heating ages for basalts from central Malaita, Solomon Islands

Sample no. and location	Depth (m)	Total fusion age (Ma)	Plateau age (Ma)	^{39}Ar % of total	Isochron age (Ma)	*N*	($^{40}Ar/^{36}Ar$) Intercept ± 1σ	*J*
Kwaio Anticline								
Singgalo River								
SG7	172	124·2	123·1 ± 2·1	100·0	118·4 ± 14·2	4	327 ± 105	0·001463
SGB10	373	126·8	126·1 ± 8·5	43·6	125·6 ± 4·6	5	336 ± 143	0·001397
SGB25	889	117·0	128·2 ± 8·5	62·5	126·6 ± 17·9	3	297 ± 11	0·001529
Kwaimbaita River								
ML423	893	104·5	none developed					
ML475	2743	119·6	123·2 ± 3·0	90·4	125·1 ± 8·3	5	289 ± 34	0·001582
Kwara'ae Anticline								
Kwaiafa'a River								
KF14	315	121·6	120·0 ± 2·2	46·6	118·9 ± 4·5	4	299 ± 16	0·001397
KF36	371	127·2	120·7 ± 3·2	61·8	120·7 ± 30·6	4	313 ± 434	0·001747
KF53	31	124·6	124·9 ± 3·8	58·7	149·6 ± 48·8	5	−104 ± 1334	0·001774

Ages are reported relative to biotite monitor FCT-3 (27·55 ± 0·12 Ma), which is calibrated against hornblende Mmhb-1 (513·9 Ma, Lanphere *et al.*, 1990). Plateau ages are the mean of concordant step ages (*N*, number of steps), weighted by the inverse of their variances. Calculations use the following decay and reactor interference constants: $\lambda_\varepsilon = 0{\cdot}581 \times 10^{-10}\,yr^{-1}$, $\lambda_\beta = 4{\cdot}963 \times 10^{-10}\,yr^{-1}$; $(^{36}Ar/^{37}Ar)_{Ca} = 0{\cdot}64$, $(^{39}Ar/^{37}Ar)_{Ca} = 0{\cdot}000673$, $(^{40}Ar/^{39}Ar)_{Ca} = 0{\cdot}01$. *J* is the neutron fluence factor, determined from measured monitor $^{40}Ar/^{39}Ar$.

Sm, Pb, Th, and U, used for isotopic age corrections, are presented together with isotopic ratios in Table 4. As in our previous studies, elemental abundances determined by isotope dilution do not necessarily represent those of the bulk rocks because, for isotopic work, small chips were handpicked from the bulk rock and cleaned in acid before powdering; also, some measurements were made on strongly acid-leached splits of these powders. In addition to the basaltic lavas, a plagioclase megacryst and its host basalt (SGB21) from a sample of the 'orbicular' facies rocks were analyzed isotopically to evaluate the genetic relationship of the megacrysts and lavas.

RESULTS

^{40}Ar–^{39}Ar ages

Previous work on the OJP has revealed two distinct sets of basement ages (Fig. 3). Lavas in southern Malaita, Ramos Island, parts of Santa Isabel, at DSDP Site 289, and at ODP Site 807 all have ages that are indistinguishable, within errors, around a mean of 122 Ma (total range is 119–125 Ma). In contrast, basalts at ODP Site 803, in much of Santa Isabel and parts of San Cristobal, and ash layers at DSDP Site 288 yield ages around 90 Ma (total range is 86–94 Ma; Mahoney *et al.*, 1993; Birkhold-VanDyke *et al.*, 1996; Parkinson *et al.*, 1996; Tejada *et al.*, 1996). Compositionally similar tholeiites with ^{40}Ar–^{39}Ar ages of ~62 Ma and ~34 Ma are also present on San Cristobal (Birkhold-VanDyke *et al.*, 1996), but their relationship to the older OJP basalts is as yet unclear. Our ^{40}Ar–^{39}Ar ages for rocks from the Singgalo, Kwaimbaita, and Kwaiafa'a river sections all fall within the ~122 Ma group (Table 3). Five of the samples produced acceptable plateau ages; that is, concordant step-ages comprising >50% of the total ^{39}Ar released. An additional two samples (SGB10, KF14) gave similar plateau ages, based on slightly less than half of the total gas; one sample (ML423) produced a recoil age-spectrum pattern, from which only a minimum (integrated) age estimate could be determined. Isochron ages are concordant with plateau ages for all samples, but generally have larger uncertainties because of the small dispersion of the few step compositions. For this reason, we take the acceptable plateau ages as the best estimate of the timing of volcanism. These five ages are indistinguishable at the 95% confidence level, and provide a mean age for the entire section of 123·1 ± 1·4 Ma. There is no evidence of any significant time difference between the lowermost and uppermost lavas, from either the ^{40}Ar–^{39}Ar ages or the volcanic stratigraphy (e.g. sedimentary interbeds are almost nonexistent). Combined with previously reported ages, these results show the ~122 Ma volcanic event was widespread across the OJP, occurring at locations separated by as much as 1600 km (see Tejada *et al.*, 1996). Furthermore, the combined data now available suggest that the ~90 Ma event is not represented on Malaita.

Volcanic stratigraphy

Effects of alteration on chemical composition

Relative to many of the samples from southern Malaita and Santa Isabel studied by Tejada *et al.* (1996), the majority of the central Malaitan lavas are only weakly altered, as indicated by, for example, their relatively low (<1·5 wt %) weight loss on ignition (LOI) values (Table 1); also, only a few samples with MgO values between 7·0 and 8·5 wt % have comparatively high K_2O and Na_2O values (>0·25 and >3·00 wt %, respectively). This is consistent with Babbs' (1997) conclusion that alteration is limited mainly to clays replacing olivine and mesostasis. As a result, data for elements and oxides known to be affected by higher levels of submarine alteration, such as Na_2O, CaO, P_2O_5, Cr, Ni, Zn, Cu, and V (e.g. Bienvenu *et al.*, 1990), still show some coherence with data for more immobile elements such as TiO_2, Fe_2O_3, Al_2O_3, Nb, Y, Zr, and the lanthanide rare earths. Nevertheless, most of our petrogenetic interpretations are based on the alteration-resistant elements.

Isotopic and chemical variations

Kwaio Anticline. Previous studies have revealed two distinct, ocean-island-like isotopic groups of OJP basement lavas; at Site 807, where both groups were sampled, they are stratigraphically separated (Mahoney & Spencer, 1991; Mahoney *et al.*, 1993; Tejada *et al.*, 1996). Two stratigraphically separated, isotopically distinct groups of lavas also are present in the Kwaio Anticline (Fig. 4; Table 4). The upper stratigraphic group has initial $\varepsilon_{Nd}(t)$ = +3·8 to +3·9, $(^{87}Sr/^{86}Sr)_t$ = 0·7040–0·7042, $(^{206}Pb/^{204}Pb)_t$ = 17·71–17·85, $(^{207}Pb/^{204}Pb)_t$ = 15·47–15·49, and $(^{208}Pb/^{204}Pb)_t$ = 37·87–37·98. The stratigraphically lower group has $\varepsilon_{Nd}(t)$ = +5·4 to +6·0, $(^{87}Sr/^{86}Sr)_t$ = 0·7037–0·7039, $(^{206}Pb/^{204}Pb)_t$ = 18·12–18·40, $(^{207}Pb/^{204}Pb)_t$ = 15·51–15·53, and $(^{208}Pb/^{204}Pb)_t$ = 38·15–38·23 (Figs 4–6). Basalts of the Kwaelungga River section south of the Singgalo River (Babbs, 1997) show similar characteristics. The plagioclase megacryst of sample SGB21 has an identical isotopic composition, within error, to that of its host rock, which belongs with the lower stratigraphic group. Malaita Volcanic Group lavas in southern Malaita (Mahoney & Spencer, 1991; Tejada *et al.*, 1996) are isotopically equivalent to the upper group. Moreover, the two isotopic groups in the Kwaio Anticline are virtually indistinguishable from those of northeastern Santa Isabel (Tejada *et al.*, 1996) and similar to the upper (Unit A) and lower (Units C–G) groups, respectively, of

Table 4: Isotope ratios and isotope dilution abundances for central Malaita, Solomon Islands

Sample		$(^{87}Sr/^{86}Sr)_t$	$\varepsilon_{Nd}(t)$	$(^{206}Pb/^{204}Pb)_t$	$(^{207}Pb/^{204}Pb)_t$	$(^{208}Pb/^{204}Pb)_t$	Rb	Sr	Sm	Nd	$(^{206}Pb/^{204}Pb)_0$	$(^{207}Pb/^{204}Pb)_0$	$(^{208}Pb/^{204}Pb)_0$	Th	U	Pb
Kwaio Anticline																
Singgalo River																
SG-1	U	0·70404	+3·9	17·847	15·472	37·913	1·277	107·8	1·689	4·607	18·511	15·505	38·537	0·2772	0·0966	0·1710
SGB13	U	0·70417	+3·7				1·471	147·6	3·650	12·02						
	L	0·70415	+3·9				0·9029	121·5	1·480	3·293						
SGB17	U			17·708	15·488	37·865					18·373	15·520	38·423	0·3003	0·1174	0·2067
	L	0·70413	+3·9				0·9675	93·13	1·540	3·425						
SGB18	U			18·117	15·513	38·215					18·570	15·535	38·633	0·2217	0·1040	0·2048
	L	0·70378	+5·7				0·6878	112·5	1·439	3·253						
SGB21	P	0·70372	+5·4				0·0778	187·4	0·0388	0·1767	18·369	15·523	38·180			0·0273
SGB21	U	0·70379	+5·8	18·403	15·514	38·199	1·311	67·44	1·591	4·150	18·963	15·541	38·554	0·1290	0·0667	0·1409
SGB25	U	0·70382	+6·0	18·245	15·506	38·147	0·1820	133·3	2·116	5·993	18·466	15·517	38·351	0·1526	0·0541	0·2869
Kwaimbaita River																
ML407	U	0·70413	+5·7	18·322	15·511	38·230	1·769	100·1	2·110	5·672	18·694	15·529	38·635	0·1553	0·0467	0·1483
	L	0·70393	+5·7				0·8105	46·78	1·981	4·490						
ML475	U	0·70371	+5·6	18·352	15·526	38·178	0·3530	74·86	0·9217	2·281	18·568	15·537	38·405	0·0705	0·0219	0·1195
ML422	L	0·70378	+5·8				0·1206	94·20	1·510	3·357						
ML451	L	0·70378	+5·5				0·2478	43·10	1·264	2·633						
ML450	L	0·70413	+3·8				0·4012	76·73	1·358	2·968						
ML421	U	0·70423	+3·8	17·756	15·468	37·984	0·3208	147·3	3·488	11·34	18·156	15·488	38·206	0·2140	0·1267	0·3687
	L	0·70415	+3·9				0·0990	109·6	1·326	2·885						
Kwara'ae Anticline																
Kwaiafa'a River																
KF1	L	0·70441	+3·9				1·360	62·23	1·281	2·928						
	D	0·70446					1·210	59·28								
KF4	U	0·70414	+3·9	17·909	15·490	38·028	1·120	115·7	1·653	4·530	18·301	15·509	38·380	0·1921	0·0700	0·2090
	L	0·70415	+3·8				0·7995	81·33	1·558	3·673						

L, strongly acid-leached powder; U, unleached but chips handpicked and acid-cleaned; P, plagioclase; D, duplicate dissolution. Isotopic fractionation corrections are $^{148}NdO/^{144}NdO = 0{\cdot}242436$ ($^{148}Nd/^{144}Nd = 0{\cdot}241572$), $^{86}Sr/^{88}Sr = 0{\cdot}1194$. Data are reported relative to University of Hawaii standard values: for La Jolla Nd, $^{143}Nd/^{144}Nd = 0{\cdot}511842$; for NBS 987 Sr, $^{87}Sr/^{86}Sr = 0{\cdot}71024$. The total range measured for La Jolla Nd is $\pm 0{\cdot}000008$ ($0{\cdot}2\varepsilon$ units); for NBS 987 it is $\pm 0{\cdot}000020$ over a 1 yr period. Present-day Pb isotopic ratios are corrected for fractionation using the NBS 981 standard values of Todt *et al.* (1996); the total ranges measured for NBS 981 are $\pm 0{\cdot}012$ for $^{206}Pb/^{204}Pb$, $\pm 0{\cdot}012$ for $^{207}Pb/^{204}Pb$, and $\pm 0{\cdot}038$ for $^{208}Pb/^{204}Pb$. Within-run errors on the isotopic data above are less than or equal to the external uncertainties on these standards. Element uncertainties are in ppm; estimated uncertainties on abundances are <0·2% on Sm and Nd; <0·5% for Sr, ~1% for Rb; <2% on Th, <1% on U, and <1% on Pb. Total blanks are negligible: <3 pg for Th, <5 pg for U, 5–30 pg for Pb, <15 pg for Nd and <60 pg for Sr. $\varepsilon_{Nd} = 0$ today corresponds to $^{143}Nd/^{144}Nd = 0{\cdot}51264$; for $^{147}Sm/^{144}Nd = 0{\cdot}1967$, $\varepsilon_{Nd}(t) = 0$ corresponds to $^{143}Nd/^{144}Nd = 0{\cdot}512486$ at 120 Ma.

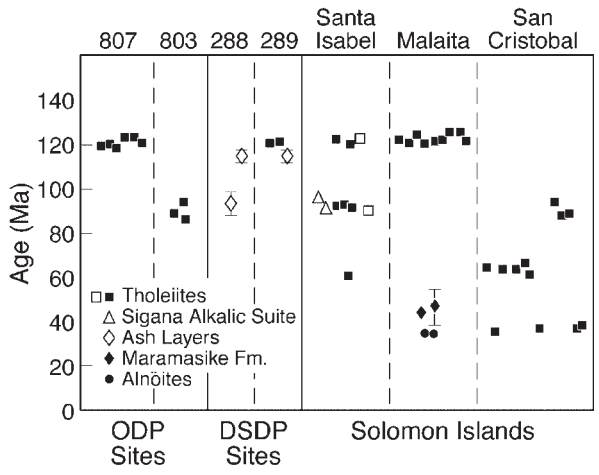

Fig. 3. Summary of ^{40}Ar–^{39}Ar and biostratigraphic (points with error bars) age data for OJP tholeiites, ash layers at DSDP Site 288, and late-stage alkalic rocks. Data sources are this paper, Davis (1978), Berger *et al.* (1993), Mahoney *et al.* (1993), Birkhold-VanDyke *et al.* (1996) and Tejada *et al.* (1996). □, mean ages reported by Parkinson *et al.* (1996).

lavas at ODP Site 807 (Mahoney *et al.*, 1993). In detail, the upper group in the Kwaio Anticline has slightly lower $\varepsilon_{Nd}(t)$ and Pb isotope ratios than the flows of Unit A at Site 807 (e.g. with $\varepsilon_{Nd}(t) = +4{\cdot}5$ to $+5{\cdot}1$), whereas the lower group possesses slightly higher $(^{87}Sr/^{86}Sr)_t$ than the Units C–G basalts (with values of 0·7034–0·7035), much like the lavas of northeastern Santa Isabel (0·7036–0·7037).

Except for compositionally extreme samples ML475 (MgO 10·0 wt %) and ML476 (MgO 5·8 wt %), the major element compositions of the Kwaio Anticline basalts have a relatively small range in MgO (6·3–8·9 wt %), molar *mg*-number [100 × Mg/(Mg + Fe^{2+}) = 51–61, assuming Fe^{2+} is 0·85 of total Fe], SiO_2 (48·6–50·5 wt %), TiO_2 (0·9–1·8 wt %), Al_2O_3 (13·5–15·9 wt %), CaO (10·4–13·2 wt %), and total Fe as Fe_2O_3 (Fe_2O_3* 11·9–14·6 wt %) (Fig. 7; Table 1). These results are consistent with those of previous studies, which have documented a much smaller range of major element variation in OJP lavas than seen in, for example, the much smaller Manihiki or Caribbean plateaux (e.g. Mahoney *et al.*, 1993; Tejada *et al.*, 1996; Kerr *et al.*, 1997). In general, lavas of the stratigraphically upper isotopic group have lower CaO and MgO/Fe_2O_3* but higher TiO_2, and Fe_2O_3* for a given MgO content than the underlying lavas (Fig. 7).

As with the two groups of lavas at Site 807, incompatible elements in the upper group of the Kwaio Anticline are slightly more abundant than in the underlying group (Tables 1 and 2): for example, TiO_2 1·5 ± 0·3 (total range) vs 1·1 ± 0·2 wt %, P_2O_5 0·14 ± 0·02 wt % vs 0·10 ± 0·02 wt %, La 5·4 ± 1·0 ppm vs 3·4 ± 0·5 ppm, Ce 14·4 ± 2·4 ppm vs 9·8 ± 0·8 ppm, Nb 5·9 ± 0·5 ppm vs 4·0 ± 1·0 ppm, and Th 0·53 ± 0·14 ppm vs 0·30 ± 0·06 ppm. Except for samples ML407, ML475, and ML476, Cr and Ni contents are generally higher in the lower group of lavas (128 ± 28 vs 112 ± 56 ppm and 110 ± 15 vs 68 ± 28 ppm, respectively), probably indicating slightly lesser amounts of crystal fractionation than in the stratigraphically upper group. Sample ML475, with 446 ppm Cr, appears to contain abundant excess (cumulus) clinopyroxene

Kwara'ae Anticline. The basalt flows exposed in the Kwara'ae Anticline are chemically very similar to the stratigraphically upper group of lavas in the Kwaio Anticline; for example, in TiO_2 (1·5 ± 0·2 wt %), P_2O_5 (0·11 ± 0·03 wt %), La (5·2 ± 1·2 ppm), Ce (15·3 ± 4·3 ppm), Nb (4·8 ± 1·3 ppm), and Th (0·48 ± 0·20 ppm; Tables 1 and 2). The two samples analyzed isotopically, KF1 and KF4, from the top and bottom, respectively, of the Kwaiafa'a River section (Figs 4–6) also have similar isotopic compositions to the upper group of Kwaio Anticline lavas, except that KF1 has higher $(^{87}Sr/^{86}Sr)_t$ (0·70441) even after multi-step acid leaching. This sample was taken from the topmost lava flow, in contact with the Kwara'ae Mudstone and separated from the rest of the lava sequence by a thin bed of chert. Its high $(^{87}Sr/^{86}Sr)_t$ value is probably a result of seawater alteration.

Proposed formation names, estimated thickness, and regional correlations

We propose that the geochemically distinct upper sequence of flows in central Malaita, characterized by lower $\varepsilon_{Nd}(t)$ and $(^{206}Pb/^{204}Pb)_t$, higher $(^{87}Sr/^{86}Sr)_t$, and greater abundances of the more highly incompatible elements, be designated as the Singgalo Formation (Fm.), and that the lower sequence, with higher $\varepsilon_{Nd}(t)$ and $(^{206}Pb/^{204}Pb)_t$, and lower $(^{87}Sr/^{86}Sr)_t$ and incompatible-element contents, be termed the Kwaimbaita Fm. These designations are appropriate because they are taken from the names of the two major rivers where the thickest exposures of each magma type have been found (Figs 2 and 4). On the basis of the close isotopic and elemental affinity noted above, ~122 Ma lavas sampled in southern Malaita, northernmost Malaita, Ramos Island, and many of those in northeastern Santa Isabel also can be classified as Singgalo type, whereas a few lavas sampled in northeastern Santa Isabel are Kwaimbaita type (Figs 5–8). Isotopic ratios of the single flow sampled at Site 289 indicate that it is also of the Kwaimbaita type. At Site 807, the upper (Unit A) and lower (Units C–G) groups of flows likewise correspond, respectively, to the Singgalo and Kwaimbaita types, although physical continuity with the Malaitan volcano-stratigraphic formations remains to be demonstrated. In contrast, the ~90 Ma lavas of

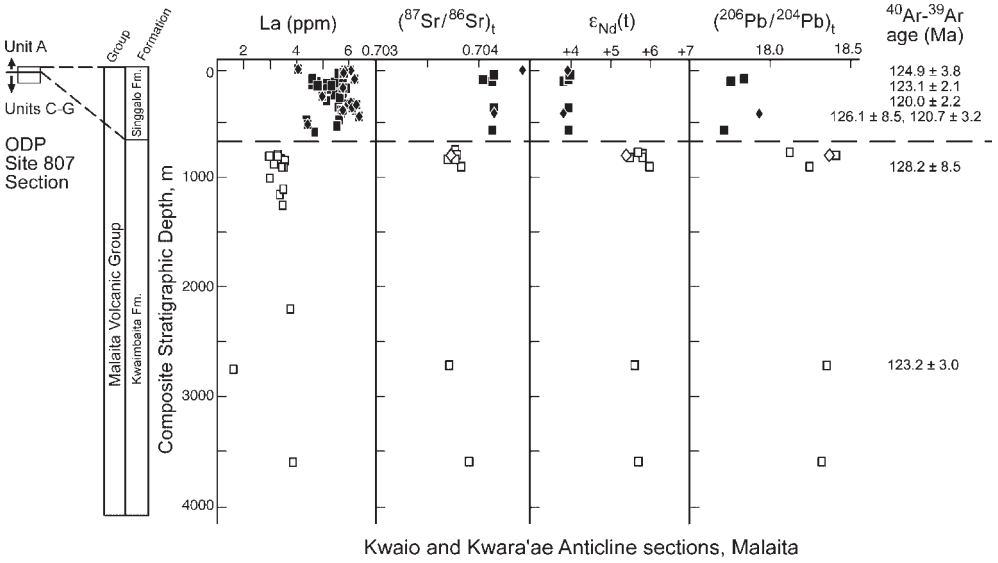

Fig. 4. Initial Pb, Sr, and Nd isotopic ratios, La content, and ^{40}Ar–^{39}Ar ages vs basement depth for central Malaita. The Site 807 basement section (e.g. Mahoney *et al.*, 1993) is shown for reference adjacent to the basement stratigraphic column in central Malaita. The filled and open symbols represent lavas of the two groups we term the Singgalo Fm. and Kwaimbaita Fm., respectively (see text); squares indicate samples from the Kwaio Anticline, and diamonds indicate samples from the Kwara'ae Anticline. The solid line in the Site 807 section represents a thin limestone unit; the bold dashed line in the central Malaitan section represents the boundary between the Singgalo Fm. and Kwaimbaita Fm; the fine dashed line correlates the equivalent boundary at Site 807.

Site 803, Santa Isabel, and San Cristobal, although isotopically similar to the ~122 Ma basalts, cannot be related directly to either formation because they are some 30 my younger; however, when discussing petrogenesis, we refer to them as Kwaimbaita-like or Singgalo-like.

Petterson (1995) estimated the maximum stratigraphic thickness of the OJP basement section exposed in central Malaita to be ~4 km. The precise determination of the thickness of the Singgalo Fm. is complicated by the presence of faults in lavas of this formation in the relevant portion of the Kwaimbaita River section and the upstream portion of the Singgalo River section (Fig. 2b). However, in the downstream portion of the Singgalo River traverse, an apparently continuous and undisturbed section exists, in which the top of the Singgalo Fm. is overlain conformably by the Kwara'ae Mudstone Fm. and the base is marked by a sharp change to Kwaimbaita Fm. isotopic and chemical compositions (Fig. 4, Table 1). The Singgalo Fm.'s thickness here is ~750 m. The Singgalo Fm. appears to be much thicker (~1290 m) in the upstream portion of the Singgalo River section, but the presence of several low-angle faults in this area (Fig. 2b) suggests a repetition of strata, which would explain why no evidence was found for a significant increase with depth in the grade of alteration (Babbs, 1997). The Singgalo Fm. section along the Kwaiafa'a River is undisturbed and ~500 m thick; however, the base of the formation is not exposed. In contrast, the thickness of the Singgalo-type flows in the basement section at Site 807 (i.e. Unit A) is only 46 m (Mahoney *et al.*, 1993; Fig. 4); furthermore, the Singgalo- and Kwaimbaita-type lava groups at this site are divided by a pelagic limestone unit of 0·5 m thickness not seen in Malaita. At Site 289, Singgalo-type lavas are missing entirely. Thus, the Singgalo magma type appears likely to be much less voluminous in the northern part of the plateau than in the south.

For the Kwaimbaita Fm. only a minimum thickness can be estimated, because its base is not exposed anywhere in the sections we sampled. From the structure of the Kwaio Anticline and the location of its fold axis (Petterson *et al.*, 1997), we estimate that the exposed thickness of the Kwaimbaita Fm. is ~2700 m in the eastern limb, where no major faults were found within this formation, and ~2600 m in the western limb (the latter value includes the 310 m exposed in the lower portion of the Singgalo River; see Fig. 2b). At Site 807, only 102 m of Kwaimbaita-type basalts (i.e. Units C–G) were penetrated before drilling was terminated.

Chemical variations within each magma type

The Malaitan lavas display a broader range of chemical composition than the basalts at Site 807, probably largely reflecting the much greater thickness of basement sampled in central Malaita. Collectively, however, data for the few, but widespread, OJP localities sampled thus far

indicate that the lavas of each magma type are compositionally very uniform overall, except for rare high-MgO examples such as ML475 and ML68, and rare evolved ones such as ML476 and the High-Ti Sigana Basalts of Santa Isabel (see Fig. 7d; Tejada *et al.*, 1996). Singgalo-type basalts can conveniently be divided into three general chemical types (Fig. 7d): (1) a high-Ti group represented by the High-Ti Sigana Basalts of Santa Isabel; (2) lavas with TiO_2 between 1·5 and 2·0 wt %, represented by Unit A at Site 807, most of the 122 Ma Sigana Basalts, and the majority of central, northern, and southern Malaitan Singgalo-type lavas; (3) basalts with TiO_2 <1·5 wt %, overlapping with Site 803 and some Kwaimbaita Fm. compositions (upper dashed outline in Fig. 7d). Similarly, Kwaimbaita-type lavas can be grouped into high- and low-Ti types: (1) those with TiO_2 between 1·0 and 1·5 wt %, representing the majority of central Malaitan Kwaimbaita Fm. lavas, the Site 807 Units C–G flows, and the Site 289 basalt; (2) those with TiO_2 $\leq$1 wt % in central Malaita (lower dashed outline in Fig. 7d). The $\sim$90 Ma Site 803 and Santa Isabel tholeiites, which are isotopically Kwaimbaita-like, are also chemically similar to the high-Ti Kwaimbaita Fm. lavas (see Tejada *et al.*, 1996).

As with Ti, relatively small variations are evident in incompatible trace element abundances within each magma type, both among flows in different locations and at a given location (Fig. 8). For example, the low-Ti Singgalo Fm. lavas of the Kwara'ae Anticline, KF1 and KF32, have lower incompatible element abundances than most other lavas in the same area (Fig. 8b). Regionally, the average incompatible element contents of the Singgalo-type basalts in central Malaita are slightly higher than the averages for southern Malaita and Santa Isabel. In addition, the Kwaio Anticline lavas have similar average abundances of highly incompatible elements (Zr to Th in Fig. 8) to those of their Site 807 counterparts, but slightly higher average abundances of moderately incompatible elements (Sm to Lu). The Kwara'ae Anticline lavas have slightly greater average abundances of most incompatible trace elements than similar units at Site 807, southern Malaita, and Santa Isabel.

Among Kwaimbaita-type basalts, a few central Malaitan low-Ti lavas with the lowest incompatible element abundances (i.e. with patterns at the lower boundary of the shaded band in Fig. 8c) display larger troughs at P,

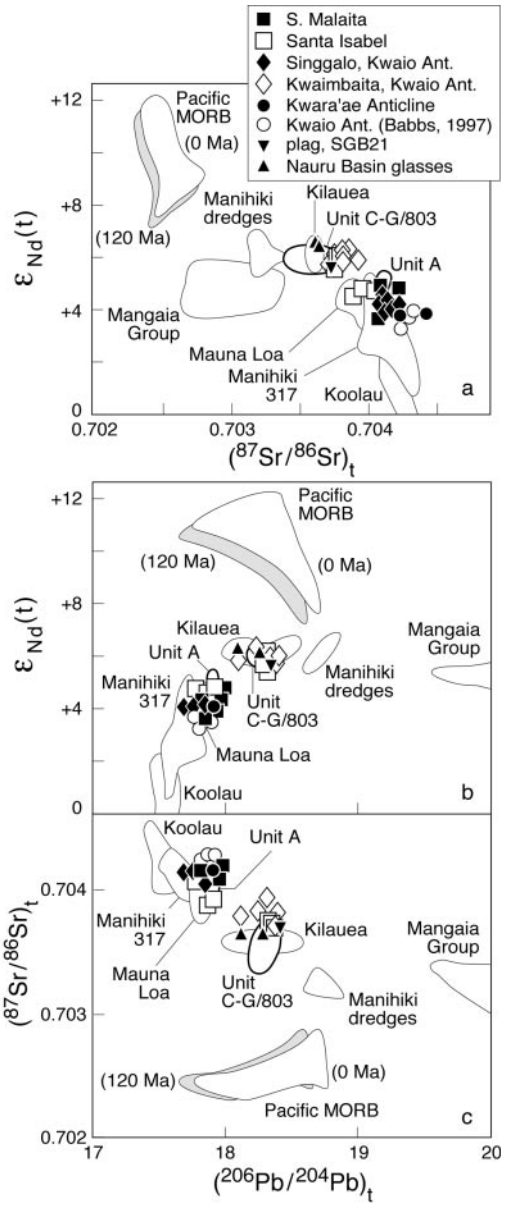

Fig. 5. Initial $\varepsilon_{Nd}(t)$ vs $(^{87}Sr/^{86}Sr)_t$ (a) and $(^{206}Pb/^{204}Pb)_t$ vs $\varepsilon_{Nd}(t)$ (b) and $(^{87}Sr/^{86}Sr)_t$ (c) for lavas of central Malaita, together with data for southern and northernmost Malaita, northeastern Santa Isabel, drill sites 289, 807 and 803 (Mahoney, 1987; Mahoney & Spencer, 1991; Mahoney *et al.*, 1993; Tejada *et al.*, 1996) and additional data from central Malaita (Babbs, 1997). The fields with bold outlines encompass the drill-site data. Also shown are fields for modern Pacific MORB (Mahoney *et al.*, 1994, and reference therein), estimated initial fields for the Manihiki Plateau (Mahoney & Spencer, 1991), and estimated initial values for glasses from the Nauru Basin (Castillo *et al.*, 1994). The shaded field adjacent to the Pacific MORB field is the estimated 120 Ma position of the MORB source mantle, assuming the only changes in the source have been radioactive decay and ingrowth. Estimated 120 Ma positions of mantle sources of selected Pacific ocean-island basalts are included: Mangaia Group (Vidal *et al.*, 1984; Palacz & Saunders, 1986; Nakamura & Tatsumoto, 1988; Chauvel *et al.*, 1992), Koolau (Stille *et al.*, 1983; Roden *et al.*, 1994), Mauna Loa (Rhodes & Hart, 1995), Kilauea (Tatsumoto, 1978; Chen *et al.*, 1996; Garcia *et al.*, 1996). The 120 Ma mantle source fields assume the following $^{87}Rb/^{86}Sr$, $^{147}Sm/^{144}Nd$, and $^{238}U/^{204}Pb$ values: 0·02, 0·24, and 5 for the MORB source (W. M. White, 1993; Mahoney *et al.*, 1998); 0·015, 0·202, and 18 for the Hawaiian source (Tatsumoto, 1978; Roden *et al.*, 1994; Garcia *et al.*, 1995); and 0·054, 0·20, and 22 for the Mangaia Group source (Chauvel *et al.*, 1992). Analytical errors on data in this study are smaller than or similar to the size of symbols.

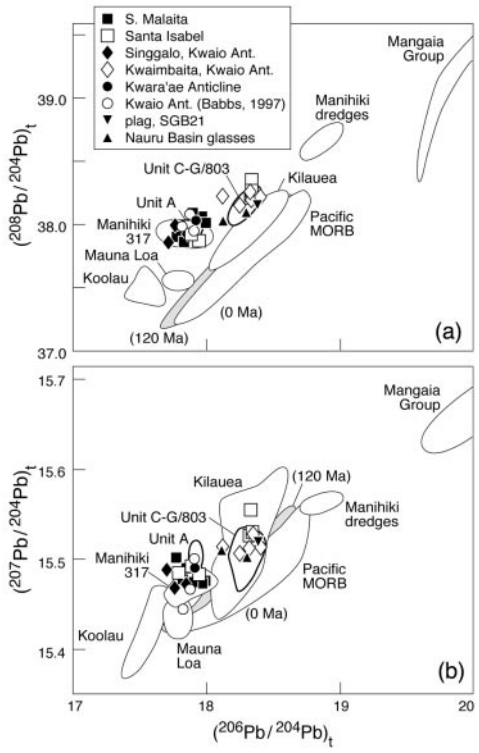

Fig. 6. Initial $(^{208}Pb/^{204}Pb)_t$ (a) and $(^{207}Pb/^{204}Pb)_t$ (b) vs $(^{206}Pb/^{204}Pb)_t$ for central Malaita, southern Malaita, and Santa Isabel basalts. Data for OJP basement drill sites are indicated by fields with bold outlines. Data sources for the other fields and mantle sources are the same as in Fig. 5. Th/U values used to adjust the mantle source fields to estimated 120 Ma positions are 2·25 for Pacific MORB (W. M. White, 1993), 3·0 for the Hawaiian source (Tatsumoto, 1978), and 3·2 for the Mangaia Group (Chauvel *et al.*, 1992). $^{238}U/^{204}Pb$ values used are as in Fig. 5. Analytical errors on $(^{208}Pb/^{204}Pb)_t$ are about the size of the symbols and those on $(^{207}Pb/^{204}Pb)_t$ are about twice the height of the squares.

Ti, and Y relative to others from the Kwaio Anticline. However, the incompatible element patterns of the Units C–G flows at Site 807, the Site 289 basalt, and most Santa Isabel flows are similar to those of most central Malaitan Kwaimbaita Fm. lavas. With the exception of evolved sample ML476, Kwaimbaita-type lavas exhibit either no peak or a variably positive peak at Sr, in contrast to the trough at Sr seen for all Malaitan Singgalo Fm. lavas.

DISCUSSION

Bimodal ages and emplacement rates

The combined age data now available for the plateau provide no evidence of a lateral age progression and thus an Icelandic-type origin by progressive lateral accretion. Instead, data for the widely separated drill-hole and island basement lavas reveal a strongly bimodal distribution of ages, at ~122 Ma and ~90 Ma (Fig. 3). For the older event, the total range of ^{40}Ar–^{39}Ar ages (excluding those for samples SGB10 and SGB25, which have large uncertainties; Table 3) is 119–125 Ma, yielding a maximum possible duration of 6 my for this event. Table 5 lists estimates of the average emplacement rates, or magmatic fluxes, corresponding to maximum and minimum OJP volumes estimated by Coffin & Eldholm (1994) and Neal *et al.* (1997), the smaller value assuming that the plateau was emplaced entirely in an off-ridge setting and the larger assuming, unrealistically, that all emplacement took place at a mid-ocean ridge. Assuming that the ~90 ± 4 Ma event recorded in lavas at Site 803, Santa Isabel, and San Cristobal and in ash layers at Site 288 was volumetrically negligible and that essentially the entire plateau was emplaced in 6 my between 119 and 125 Ma gives minimum average emplacement rates of 4·5–10·2 km^3/yr. These values are at the low end of previous estimates of 16–20 km^3/yr (which assumed a duration of only 3 my; Coffin & Eldholm, 1994) and 8–22 km^3/yr (assuming a duration of 3 my and an OJP volume of 24×10^6 to 65×10^6 km^3; Tarduno *et al.*, 1991).

However, besides the 90 ± 4 Ma event, the recognition of OJP-related lavas with ages of ~111–115 Ma covering extensive areas in the Nauru and East Mariana basins (e.g. Castillo *et al.*, 1994) may suggest a lower overall average emplacement rate (see also Ito & Clift, 1998; Ito & Taira, 2000). Assuming that the 90 ± 4 Ma event was volumetrically important, was characterized by similar eruption rates to those of the ~122 Ma event, and that magmatism in the period between 94 and 119 Ma was minor, the maximum total duration of plateau emplacement in the two eruptive events would be 14 my and the minimum average emplacement rates would have been 1·9 km^3/yr and 4·4 km^3/yr for off- and on-ridge settings, respectively. These values are similar to maximum estimates for the Kerguelen Plateau (3·4–5·4 km^3/yr; Coffin & Eldholm, 1994) but still much higher than estimates for other large igneous provinces. For average emplacement rates to fall as low as values estimated for the Deccan Traps (0·3–2·4 km^3/yr; Coffin & Eldholm, 1994), North Atlantic Tertiary Province (0·6–2·4 km^3/yr; Coffin & Eldholm, 1994), or Shatsky Rise's South High (1·7 km^3/yr; Sager & Han, 1993), for example, the observed bimodal age distribution on the OJP would have to be an artifact of the few basement locations currently sampled, such that additional pulses or relatively continuous volcanism occurred in the 86–126 Ma period, possibly for up to 39 my. In the latter case, the estimated minimum average emplacement rates would fall to 0·7 and 1·6 km^3/yr. If the geochemically OJP-like volcanism in the East Mariana Basin ($0{\cdot}25 \times 10^6$ km^3) and Nauru Basin ($0{\cdot}85 \times 10^6$ km^3) is included,

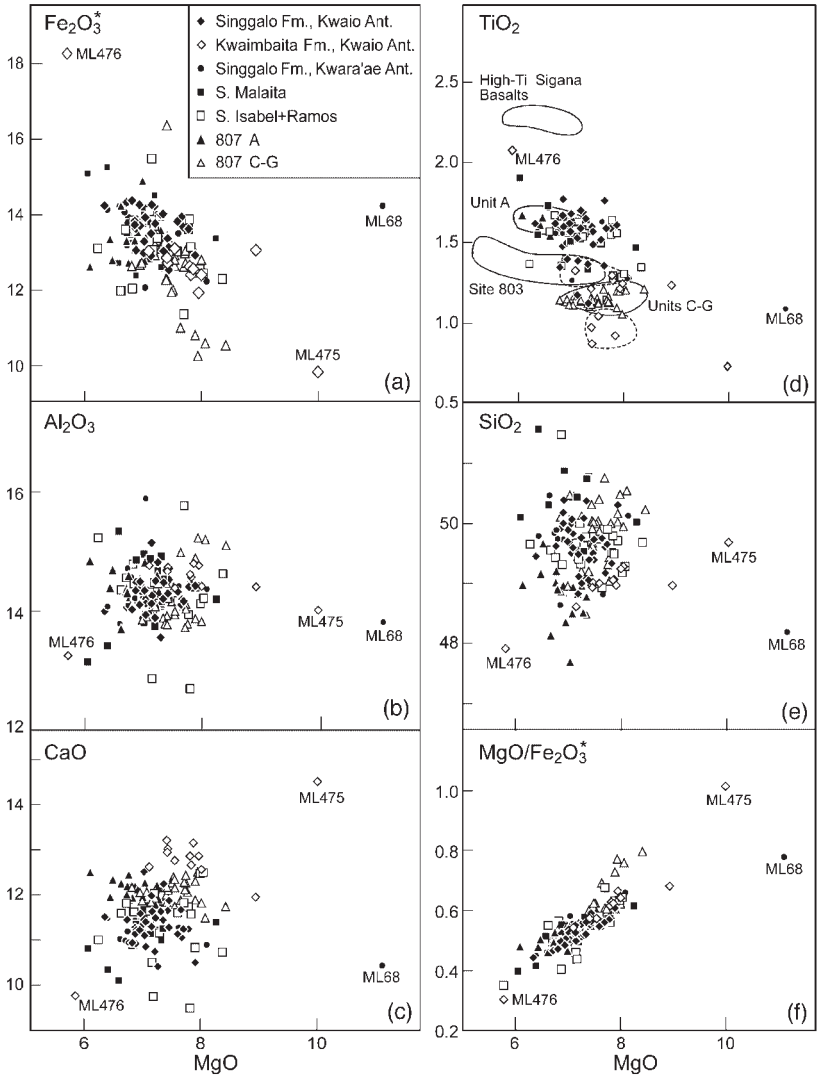

Fig. 7. Major element oxides vs MgO (wt %) comparing data for central Malaita with those of southern Malaita, Santa Isabel, and the drill sites. Symbols are as in Figs 5 and 6. Sample ML68 is a basalt (Singgalo type, as determined by its isotopic ratios) from northernmost Malaita (Tejada *et al.*, 1996). The four chemical sub-types of lavas from the drill sites, southern Malaita and northeastern Santa Isabel (Mahoney *et al.*, 1993; Tejada *et al.*, 1996) defined previously on the basis of TiO_2 contents are indicated in (d) by continuous outlines: A-type, C–G-type, 803-type, and high-Ti Sigana (data for Site 803 and high-Ti Sigana basalts not shown). The dashed outlines in (d) indicate two newly recognized magma types: low-Ti Singgalo Fm. lavas (upper field) and low-Ti Kwaimbaita Fm. (lower field).

the estimated total crustal volume associated with the OJP for off-ridge and on-ridge emplacement increases to $28{\cdot}1 \times 10^6$ (Neal *et al.*, 1997) and $62{\cdot}4 \times 10^6$ km^3 (Coffin & Eldholm, 1994), respectively. In this case, the average emplacement rates would vary from 1·6 to 3·5 km^3/yr if magmatism were episodic (total of 6, 4, and 8 my duration in the ~122, ~111–115, and ~90 Ma events). The ~62 and ~34 Ma events documented in San Cristobal (Birkhold-VanDyke *et al.*, 1996; Birkhold *et al.*, in preparation) provide evidence of an unknown amount of compositionally OJP-like tholeiitic basalt magmatism younger than ~90 Ma. We also note that an unknown volume of crust was added to the plateau at ~44 Ma, as recorded in the alkalic Maramasike Fm. of Malaita (Tejada *et al.*, 1996). If the extent of any of these events turns out to have been significant, then estimates of overall average emplacement rates would be reduced further.

Estimates of average emplacement rates will improve as more samples, ^{40}Ar–^{39}Ar dates, and crustal thickness

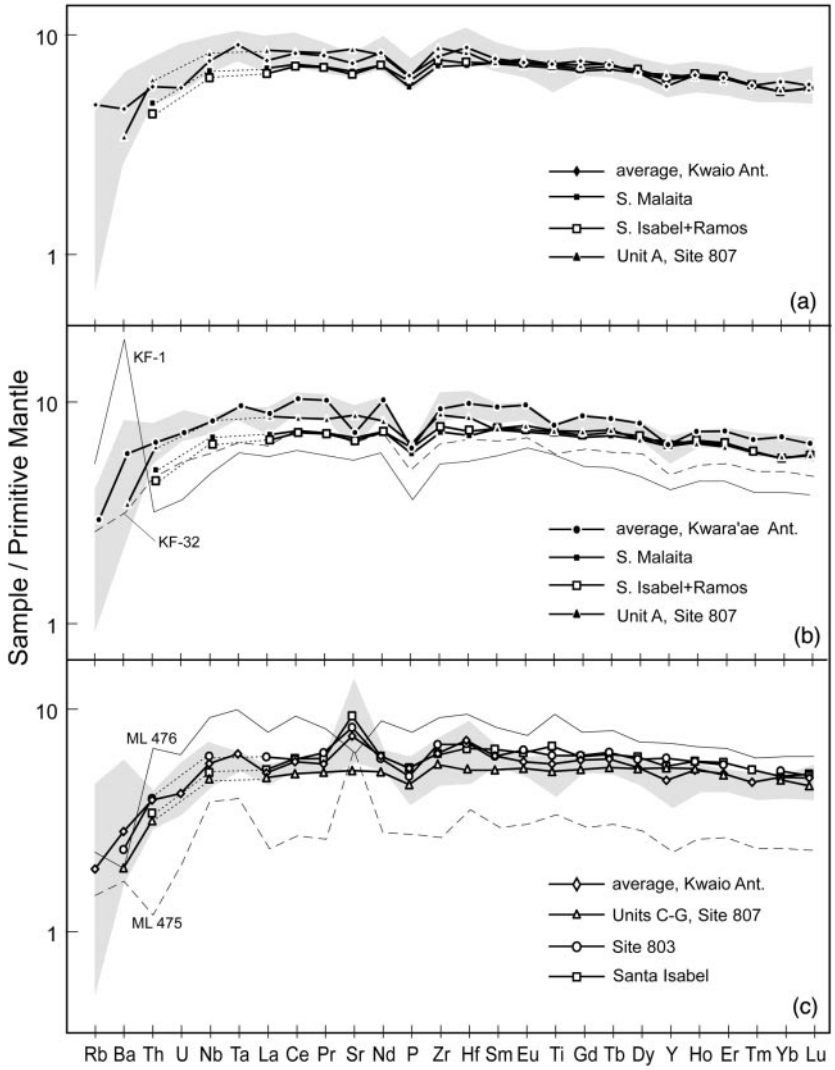

Fig. 8. Comparison of the primitive-mantle-normalized incompatible element abundances of Singgalo-type lavas with Singgalo Fm. lavas of the Kwaio Anticline (a) and Kwara'ae Anticline (b), and of Kwaimbaita-type lavas with Kwaimbaita Fm. lavas of the Kwaio Anticline (c) showing averages and total ranges (shaded envelopes). The average and range for the Kwara'ae Anticline data exclude low-Ti samples KF1 and KF32. Kwaimbaita Fm. average and range exclude ML475 and 476. Average patterns for Singgalo-type lavas of Site 807, southern Malaita, and northeastern Santa Isabel are shown in (a) and (b), whereas average patterns for Kwaimbaita-type lavas from Site 807, Site 803, and northeastern Santa Isabel are shown in (c). Normalizing values are from McDonough & Sun (1995).

data become available but, so far, all estimates are much higher than those calculated for modern hotspots such as Iceland and Hawaii (0·12–0·24 km^3/yr and 0·03–0·16 km^3/yr, respectively; R. S. White, 1993). Present indications are that the contribution of post-90 Ma magmatism to the plateau's volume was relatively minor (Mahoney *et al.*, 2002). If further sampling confirms that the bulk of the OJP was formed at ~122 Ma or in two events at ~122 and ~90 Ma, it will be difficult to avoid the conclusion that the OJP represents melting of mantle on a scale not seen in either modern hotspots or other large igneous provinces.

Petrogenetic implications of chemical variations

Phase equilibria and possible fractionation paths from multiple parental melts

Major element compositions of the majority of OJP lavas coincide approximately with the low-pressure cotectic,

Table 5: Average estimated minimum emplacement rates for the Ontong Java Plateau

Volume (km^3)		Age (Ma)	Maximum duration (my)	Emplacement rates (km^3/yr)		Assumption
Minimum[a] (off-ridge)	Maximum[b] (on-ridge)			Minimum (off-ridge)	Maximum (on-ridge)	
$27{\cdot}0 \times 10^6$	$61{\cdot}3 \times 10^6$	119–125	6	4·5	10·2	One volcanic event for the whole plateau
$27{\cdot}0 \times 10^6$	$61{\cdot}3 \times 10^6$	86–125	39	0·7	1·6	Continuous eruption from 122 Ma event to 90 Ma event
$27{\cdot}0 \times 10^6$	$61{\cdot}3 \times 10^6$	119–125 +86–94	14	1·9	4·4	Two episodic events at 122 Ma and 90 Ma
$28{\cdot}1 \times 10^6$	$62{\cdot}4 \times 10^6$	119–125 +111–115 +86–94	18	1·6	3·5	Episodic 122 Ma and 90 Ma events, plus 111–115 Ma Nauru Basin and East Mariana Basin event

Volume estimates are from [a]Neal *et al.* (1997) and [b]Coffin & Eldholm (1994).

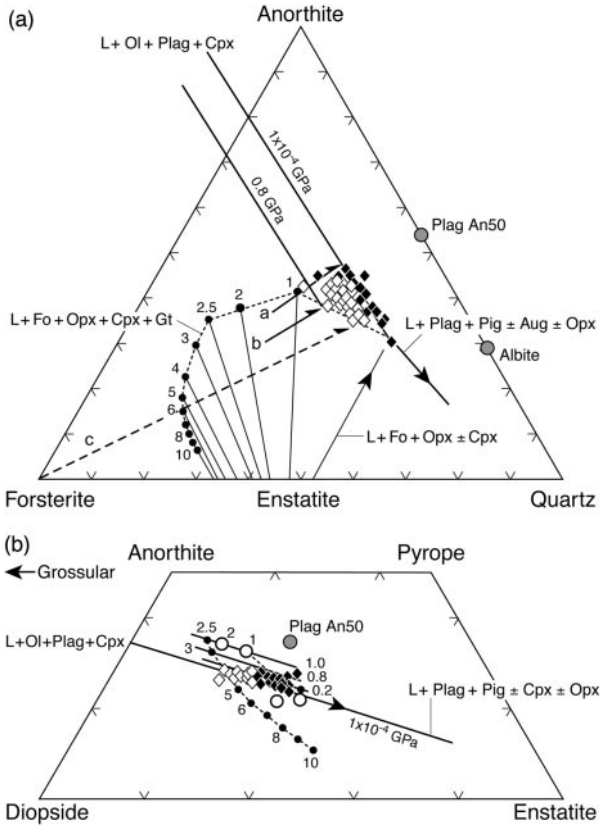

Fig. 9. (a) A projection of OJP data from diopside into the plane olivine–anorthite–quartz, assuming $Fe^{3+}/Fe^{2+} = 0{\cdot}15$, together with experimental data represented by lines with dots at the ends (Herzberg & O'Hara, 1998, and references therein). The broken lines connecting the dots are the trace of liquids formed by invariant melting of plagioclase, spinel, and garnet lherzolites at the pressures indicated in GPa. All OJP data project between the 1×10^{-4} GPa (1 atm) cotectic [Liq + ol + plag + cpx] of Libourel *et al.* (1989) and the 1×10^{-4} to 1 GPa initial melt track. The 0·8 GPa cotectic [Liq + ol + plag + cpx] is from Grove *et al.* (1992). Continuous lines with half-arrows labeled a and b demonstrate the effect of olivine fractionation. The dashed line with half-arrowhead labeled c represents inferred olivine-controlled fractionation responsible for some OJP lavas. (b) A projection of the OJP data from olivine into the plane $CaSiO_3$–$MgSiO_3$–Al_2O_3 (Herzberg & O'Hara, 1998), which contains pyroxenes and garnet. Lines labeled 0·2, 0·8, and 1·0 are cotectics [Liq + ol + plag + cpx] at the pressures indicated in GPa (Grove *et al.*, 1992). ○, invariant points at 1×10^{-4}, 1, and 2 GPa from Longhi (1987) and Walter & Presnall (1994).

liquid + olivine + plagioclase + clinopyroxene, consistent with the mineral phases observed and the ophitic to subophitic texture of clinopyroxene and plagioclase in the phyric lavas. The differentiation trajectories (arrows a–c) in Fig. 9a illustrate olivine-controlled fractionation trends. The spread of data between the 1×10^{-4} GPa (1 atm) and 0·8 GPa (8 kbar) cotectics (Fig. 9a and b) demonstrates the importance of crustal-level fractionation processes.

OJP lavas also may be inferred to be derivative liquids that have undergone significant olivine fractionation at

greater pressures; yet we do not see direct evidence for such fractionation because the effects of low-pressure fractionation effectively dominate the major element signature of the lavas (see Neal *et al.*, 1997). Although some Kwaimbaita lavas may have differentiated from ~1 GPa melts (arrow a in Fig. 9a), the majority of the data appear to fall at the ends of olivine-control trajectories originating from melts formed between 1 and 4 GPa (arrow b). Interestingly, trace element modeling also requires 3·5–4·0 GPa initial melting pressures to fit the OJP data (Tejada, 1998; see also Mahoney *et al.*, 1993; Neal *et al.*, 1997). In any case, the diagram indicates that, if they formed from peridotite source mantle, the erupted OJP lava compositions are significantly different from primary magma compositions (e.g. Herzberg & O'Hara, 1998).

Some data for Singgalo-type lavas fall at the end of the 4–6 GPa olivine-control trend (dashed arrow c is the 6 GPa olivine control), similar to most Hawaiian lavas (Herzberg & O'Hara, 1998). Although this type of diagram, derived from isobaric experimental data, provides only a rough idea of equilibration pressures of polybaric natural melts, the similarity with Hawaiian tholeiites is perhaps not too surprising considering that the Singgalo Fm. was erupted at the end of the 122 Ma episode, when the lithosphere of the OJP had probably been thickened significantly by the emplacement of the earlier Kwaimbaita-type magmas, cumulates, and melt-depleted residues. A deeper origin for Singgalo-type magmas is also consistent with trace element modeling suggesting higher initial pressures of melting for Singgalo-type magmas (Tejada, 1998).

Another important indication of polybaric fractionation is given by the Al:Ti ratios measured in clinopyroxene, present both as a phenocryst and groundmass phase, in lavas from central and northern Malaita. Values range between 4 and 10, implying pressures of formation from $\sim 1 \times 10^{-4}$ GPa (~1 atm) to a maximum of 1 GPa (Babbs, 1997). This finding is consistent with the position in Fig. 9 of the bulk of the whole-rock major element data, which fall between the 1×10^{-4} GPa and 0·8 GPa cotectics.

Source variation vs melting processes

Among the major elements (Fig. 7), TiO_2, P_2O_5 (not shown) and, to a lesser extent, Fe_2O_3* show a clear distinction between Kwaimbaita-type and Singgalo-type lavas at similar *mg*-number. This difference could potentially reflect the composition of the mantle sources or be a result of differences in the amounts and/or pressures of partial melting. TiO_2, for example, is sensitive to the amount of partial melting (e.g. Hirose & Kushiro, 1993), behaving as an incompatible element during mantle melting and attaining the highest concentrations in small-degree partial melts. The lower concentrations of TiO_2 in the Kwaimbaita-type lavas at a given *mg*-number suggest larger fractions of partial melting than for the Singgalo-type basalts. Previous major and trace element modeling indicates that both groups of rocks were formed by large total amounts of partial melting (most estimates are in the 18–30% range, assuming peridotite sources), but suggest that the Kwaimbaita basalts represent several percent more melting (Tejada *et al.*, 1996; Neal *et al.*, 1997; Tejada, 1998).

Alternatively, can the difference in chemical compositions between the Kwaimbaita and Singgalo magma types be a function of source differences? The values for many incompatible element ratios among rocks from different locations on the OJP overlap, particularly when interlaboratory variation and variable analytical precision are considered. In diagrams involving ratios of elements with significantly different bulk partition coefficients and having higher analytical precision, such as Ce/Sm, Zr/Nb, Gd/Yb, and Zr/Y (Fig. 10b, c, e and f), a weak correlation with La abundance is observed. On the other hand, ratios of elements with similar incompatibilities, such as La/Nb and Nb/Th (Fig. 10a and d), show no clear covariation with La (or with isotopic ratios). This observation is consistent with both the generally similar shapes of primitive-mantle-normalized incompatible element patterns for Singgalo- and Kwaimbaita-type lavas (Fig. 8) and the generally slightly higher abundances of incompatible elements in the Singgalo-type lavas, and probably reflects slightly lower degrees of melting for the latter. Because ratios of incompatible trace elements with similar incompatibilities, such as Nb/Th, and La/Nb, are not changed significantly by moderate amounts of magmatic differentiation or by variations in melt fraction at large total amounts of partial melting, they must mainly reflect the extent of variation in mantle source regions. Figure 10a and d suggests that although the sources of OJP lavas had distinct isotopic compositions, they had very similar ratios of highly incompatible trace elements (see also Neal *et al.*, 1997).

Bimodal isotopic compositions: a vertically zoned mantle source for the OJP?

The combined isotopic data now available indicate that a mantle source containing material of two distinct compositions, the Singgalo and Kwaimbaita types, dominated magma production, at least for the later stages of volcanism represented by basalts in the upper few kilometers of OJP crust. Importantly, there is no evidence of either magma or source mixing between the two types during the ~122 Ma event. It should be noted that the bimodal distribution of data on the Pb–Pb isotope diagrams (Fig. 6) was less sharply defined in previous studies because most Pb isotope ratios were not age-corrected (the age-corrected Pb isotopic data in Table 4 are the first for

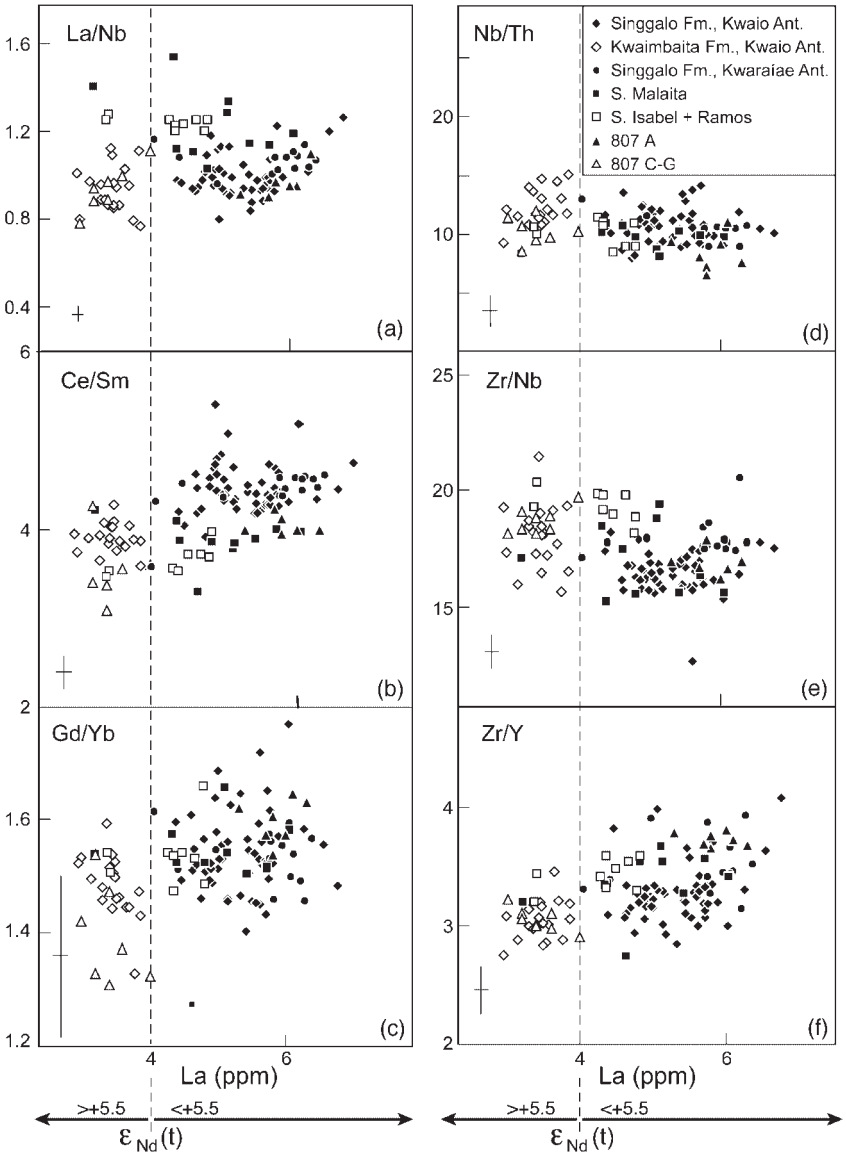

Fig. 10. Selected incompatible element ratios vs La and $\varepsilon_{Nd}(t)$. The $\varepsilon_{Nd}(t)$ value of 5·5 approximates the boundary between the two chemical types (also see Fig. 4). Fine dashed lines separate data for the Singgalo and Kwaimbaita formations and error bars represent typical analytical uncertainties for data of this study.

which parent and daughter nuclides were both measured on the same sample splits by isotope dilution).

A two-component mantle source also has been inferred, for example, for the Hawaiian hotspot, currently the world's most active, with end-members represented by shield lavas of Kilauea and Koolau volcanoes (e.g. Rhodes & Hart, 1995; Chen *et al.*, 1996). Intriguingly, the Kwaimbaita and Kilauea isotopic ranges overlap significantly (Figs 5 and 6). Koolau values range to lower ε_{Nd} and $^{206}Pb/^{204}Pb$ than yet found for the OJP but Singgalo-type isotopic values are close to, or overlap with, those for historical lavas of Mauna Loa volcano, except that the Mauna Loa lavas have lower $^{207}Pb/^{204}Pb$ and, particularly, $^{208}Pb/^{204}Pb$.

The geochemical stratigraphy in central Malaita and at Site 807 indicates a temporal change in the composition of the OJP mantle source. At Mauna Loa volcano, a somewhat similar shift from earlier (i.e. in the prehistoric lavas) Kilauea-like to more 'typical', lower-$^{206}Pb/^{204}Pb$ and lower-ε_{Nd} Mauna Loa compositions in the historical lavas (Kurz *et al.*, 1995) coincided with declining magma production (Moore *et al.*, 1990). The analogy for the OJP is limited, however, because the different Hawaiian shield volcanoes and/or lava sequences within a single shield

appear to represent different amounts of mixing between the two end-member components, whereas no mixing between Kwaimbaita- and Singgalo-type sources or magmas is observed in the ~122 Ma lavas. Rather, the shift from Kwaimbaita-type to Singgalo-type compositions is abrupt in the two locations where it has been found (i.e. Site 807 and Malaita). The lack of intermixtures between the two OJP isotopic groups, their consistent stratigraphic position in lavas emplaced at essentially the same time in two locations ~1600 km apart, and the probably small amount of drift of the plateau during the 125–100 Ma period (Neal *et al.*, 1997) suggest that the two mantle reservoirs in the OJP source were much larger in size than the scale of melting and, in the melting region, may have been vertically separated from one another.

Modeling the OJP's mantle source

In recent years, most attempts to explain large igneous provinces have invoked mantle plumes. An exception is the plate reorganization model (e.g. Anderson *et al.*, 1992; Smith & Lewis, 1999), in which flood basalt volcanism is initiated by plate reorganization above anomalously hot, shallow, non-plume mantle. Initially, melting is assumed to tap a hypothesized widespread, shallow mantle layer with ocean-island-like isotopic and trace element characteristics [termed the 'perisphere' by Anderson (1996)]; this layer is later replaced by upwelling mid-ocean ridge basalt (MORB)-type mantle that lies beneath it. The model thus predicts that MORB-like isotopic compositions should dominate the signature of late-stage lavas on oceanic plateaux. Although the OJP's ~122 Ma event, in particular, occurred relatively close in time to a major reorganization of the Pacific plate (Neal *et al.*, 1997), the complete absence, thus far, of isotopically MORB-like lavas in the ~122 Ma (and ~90 Ma) OJP crustal section does not support the plate reorganization model. Rather, the Singgalo Fm. lavas are even less MORB-like than the earlier Kwaimbaita Fm. basalts.

Another class of model posits that oceanic plateaux are formed gradually over tens of millions of years by more or less steady-state, ridge-centered or near-ridge plumes, rather like the comparatively small Icelandic Plateau or Galápagos Platform and its associated aseismic ridges (e.g. Mahoney & Spencer, 1991; Ito & Clift, 1998). Here, involvement of MORB-type mantle also might be expected, particularly in locations distant from the plume center. Perhaps more importantly, this model finds no support in the currently available age data for OJP basement lavas, which indicate that eruption occurred in short-lived pulses ~30 my apart.

By far the most frequently applied plume-based model for large igneous provinces in the last decade has been the starting-plume or plume-head model (e.g. Richards *et al.*, 1989; Griffiths & Campbell, 1990). Some laboratory and numerical experiments suggest that, for all but the largest plume heads, significant amounts of ambient, mostly lower mantle may be entrained during the ascent of a plume head from a thermal boundary layer within the mantle, possibly from the core–mantle boundary, and therefore plume heads are predicted to be compositionally zoned or layered (e.g. Griffiths & Campbell, 1990). Thus, in open-ocean areas such as that in which the OJP formed (e.g. Neal *et al.*, 1997), where complications arising from a plume's interaction with continental lithosphere are absent, the isotopic compositions of the volcanic products are predicted to reflect the plume-source and some amount of entrained lower mantle. The different ocean-island-like isotopic compositions of the OJP lavas are not inconsistent with these predictions, as the Singgalo- and Kwaimbaita-type isotopic groups would represent internally homogeneous (relative to the scale of melting) mantle regions composed of slightly different proportions of plume-source mantle and entrained, presumably lower, mantle.

Although interpretation is very model-dependent, the Kwaimbaita-type basalts in the framework of this class of models would more probably reflect the greater amount of plume-source-derived mantle. First, both in central Malaita and at Site 807, the thickness of the earlier, Kwaimbaita-type lavas is much greater than that of the later, Singgalo-type lavas, which appears consistent with laboratory and numerical models that suggest large plume heads will contain much more plume-source material than entrained mantle (e.g. Griffiths & Campbell, 1990). Second, the chemical compositions of Kwaimbaita-type basalts indicate derivation by somewhat larger amounts of partial melting of peridotite, consistent with hotter, plume-source-dominated mantle (see above). Third, the ~90 Ma eruptive event, which may have been centered on the plateau's eastern lobe or salient (Tejada *et al.*, 1996; Neal *et al.*, 1997), produced lavas with Kwaimbaita-like compositions at Site 803, Santa Isabel, and San Cristobal, whereas ~90 Ma Singgalo-type lavas have been found only in San Cristobal. Fourth, the 111–115 Ma Nauru, East Mariana, and Central Pacific Basin basalts, which appear to be closely related to emplacement of the OJP, have isotopic ratios that overlap with those of the Kwaimbaita Fm. (e.g. Figs 5 and 6). Thus, the Kwaimbaita-type signature appears to be expressed much more commonly than the Singgalo type, suggesting that the former was volumetrically more abundant in the OJP mantle source.

However, several critical aspects of the OJP do not obviously conform to the starting-plume model (see also Mahoney *et al.*, 1993; Tejada *et al.*, 1996; Neal *et al.*, 1997; Sheth, 1999). The model predicts rapid emplacement in a single event; for the OJP this would require that the

~90 Ma event was volumetrically negligible and caused by magmatism related to the plume tail that followed the plume head. At present, the magnitude of the ~90 Ma episode remains unknown, but it was clearly widespread, showing up in locations as far apart as Site 803, Site 288, San Cristobal, and Santa Isabel. Also, plume-tail-related volcanism following the plume-head phase is predicted to form a post-plateau chain of seamounts adjacent to a plateau as plate motion moves the plateau away from the hotspot, but the seafloor adjacent to the OJP lacks a post-90-Ma chain; if one ever existed, it must have been obliterated by subduction along the old Solomon trench. Recent numerical modeling suggests that a different type of large plume head may form at mid-mantle depths beneath the 660 km discontinuity, rather than above it or the core–mantle boundary (Cserepes & Yuen, 2000). Such plume heads may not be accompanied by very long-lived tails (D. Yuen, personal communication, 1999); if so, this model may account for the lack of a post-OJP seamount chain. However, this and other plume-head models also predict that substantial uplift accompanies plateau emplacement, with large areas at shallow depths or even emergent; yet paleodepths appear never to have been shallow at any of the locations sampled thus far in Malaita, Santa Isabel, or at any of the drill sites (e.g. Neal *et al.*, 1997; Ito & Clift, 1998; Michael, 1999; Ito & Taira, 2000; Mahoney *et al.*, 2002). Furthermore, if the ~90 Ma event was relatively minor, a truly enormous plume head is required to fuel melting of peridotite at a rate and volume capable of building the huge OJP in only a few million years or less at ~122 Ma (e.g. Coffin & Eldholm, 1994).

More recently, several studies have modified the starting-plume model by proposing that plume heads, although consisting principally of peridotite, may contain significant amounts of embedded eclogitic material derived from subducted oceanic crust (e.g. Cordery *et al.*, 1997; Yasuda *et al.*, 1997). The idea behind this 'composite diapir' model is that the eclogite melts extensively before the peridotite begins to melt, but cannot escape the source until peridotite melting allows large-scale melt connectivity, at which point large volumes of melt may be released cataclysmically. Yasuda *et al.* (1997) showed that the major element compositions of hybrid magmas derived by melting of such mixed sources could be comparable with those of continental flood basalts, implying that some flood basalts could be near-primary magmas.

Intra-oceanic plateaux such as the OJP should be the best places to test the composite diapir model using isotopes, trace elements, and major elements, because direct continental lithospheric influence on magma compositions is lacking. Because subducted, recycled oceanic upper crust is expected to develop high $^{206}Pb/^{204}Pb$ ratios on time scales of $\sim 10^8$ yr (e.g. Kogiso *et al.*, 1997), the plume peridotite assumed to surround pockets of recycled crust must have Pb isotopic values as low as or lower than observed in the OJP basalts. Figure 11a–d illustrates that it is indeed possible to approximate the OJP's isotopic characteristics by mixing 0·5–20% partial melts of peridotite, assumed here for simplicity to have model primitive-mantle isotopic and elemental compositions, with a 100% melt of recycled upper oceanic crust (eclogite), the isotopic characteristics of which have been modified by seafloor aging and subduction-related dehydration processes (see Table 6 for the model compositions used in constructing Fig. 11). The calculations show that an 80–98% proportion of eclogite melt is required to broadly reproduce the $^{206}Pb/^{204}Pb$, Nd, and Sr isotopic values of OJP lavas if the plume-source peridotite melts only to a very small extent (0·5%), consistent with Cordery *et al.*'s (1997) 'best' melt volume scenario. However, the amount of peridotite partial melting that accompanies complete melting of the eclogite generally might be expected to be somewhat higher, considering that the eclogite itself ultimately represents MORB-type crust formed by at least several percent of partial melting of (non-plume) peridotite. If the plume-source peridotite melts to a greater extent (e.g. 20% in the example illustrated in Fig. 11), a smaller proportion (only 40–60% in the example) of recycled oceanic upper crust can produce the OJP isotopic compositions. In all cases, with the primitive-mantle and eclogite Pb isotope values used for the figure, the $^{207}Pb/^{204}Pb$ ratios of the postulated hybrid magmas are much lower than observed for the OJP lavas for any given $^{206}Pb/^{204}Pb$ value. Of course, the plume peridotite need not have primitive-mantle isotopic (or elemental) values; a more EM-1-like end-member, for example, provides higher relative $^{207}Pb/^{204}Pb$ and still yields reasonable fits in Fig. 11a–d. Even if the plume peridodite is primitive mantle, this may not present much of a problem because of the large uncertainties in, and the large range of, estimates of primitive-mantle Pb isotopic ratios (dashed field in Fig. 11e; e.g. Galer & Goldstein, 1996).

Model incompatible element patterns generated by mixing batch melts of primitive mantle and recycled oceanic crust are shown in Fig. 12. Patterns for unaltered and altered MORB modified by dehydration in a subduction zone were estimated using the trace element mobilities derived by Kogiso *et al.* (1997). The calculated mixtures do not reproduce the patterns of OJP lavas too successfully. Models assuming a purely peridotitic source give a better fit to the data (see Tejada *et al.*, 1996; Neal *et al.*, 1997; Tejada, 1998). In particular, the patterns of OJP lavas lack the U and Rb enrichment expected for altered, recycled MORB and have different overall shapes than the model patterns. Slightly better fits are achieved if the recycled crust is assumed to be unaltered when subducted and dehydrated. Although none are very good, the best fits are obtained with ~100% melting of recycled

Table 6: Isotope systematics for one model of recycled oceanic crust (eclogite) and model primitive mantle in the OJP plume source

		$^{206}Pb/^{204}Pb$	$^{207}Pb/^{204}Pb$	$^{208}Pb/^{204}Pb$	$^{87}Sr/^{86}Sr$	$^{143}Nd/^{144}Nd$	ε_{Nd}
MORB values at $t = 0$		18·637	15·505	38·126	0·70266	0·51311	+9·1
MORB source at $t = 300$ Ma	P/D	5	0·04	12·5	0·02	0·24	
	Initial ratios	18·40	15·49	37·94	0·70257	0·51264	+7·5
MORB crust after 100 my	P/D	11	0·08	29·9	0·018	0·215	
(unaltered)	Ratios	18·57	15·5	38·09	0·7026	0·51278	+7·7
Recycled MORB at 120 Ma	P/D	103	0·75	123·6	0·195	0·264	
(altered)	Ratios	19·86	15·56	38·58	0·70282	0·51291	+8·4
PM at $t = 0$	Ratios	17·781	15·42	38·149	0·705	0·51264	0
PM at $t = 120$ Ma	P/D	8·2	0·06	32·8	0·085	0·1967	
	Ratios	17·63	15·41	37·95	0·70486	0·51249	0
	Conc.	0·071	0·071	0·0795	19·9	1·25	

MORB, mid-ocean ridge basalt; PM, primitive mantle, P/D, parent–daughter ratios: $^{238}U/^{204}Pb$ for $^{206}Pb/^{204}Pb$, $^{235}U/^{204}Pb$ for $^{207}Pb/^{204}Pb$, $^{232}Th/^{204}Pb$ for $^{208}Pb/^{204}Pb$, $^{87}Rb/^{86}Sr$ for $^{87}Sr/^{86}Sr$, and $^{147}Sm/^{144}Nd$ for $^{143}Nd/^{144}Nd$. $\varepsilon_{Nd} = 0$ corresponds to 0·512254 at 300 Ma, 0·512383 at 200 Ma, and 0·512486 at 120 Ma. Parent–daughter values are from W. M. White (1993) and Mahoney *et al.* (1994) for southern East Pacific Rise MORB, and from Jacobsen & Wasserburg (1980), McCulloch & Black (1984) and Galer & Goldstein (1996) for primitive mantle. Concentration values and parent–daughter ratios for recycled MORB are from Kogiso *et al.* (1997) and references therein.

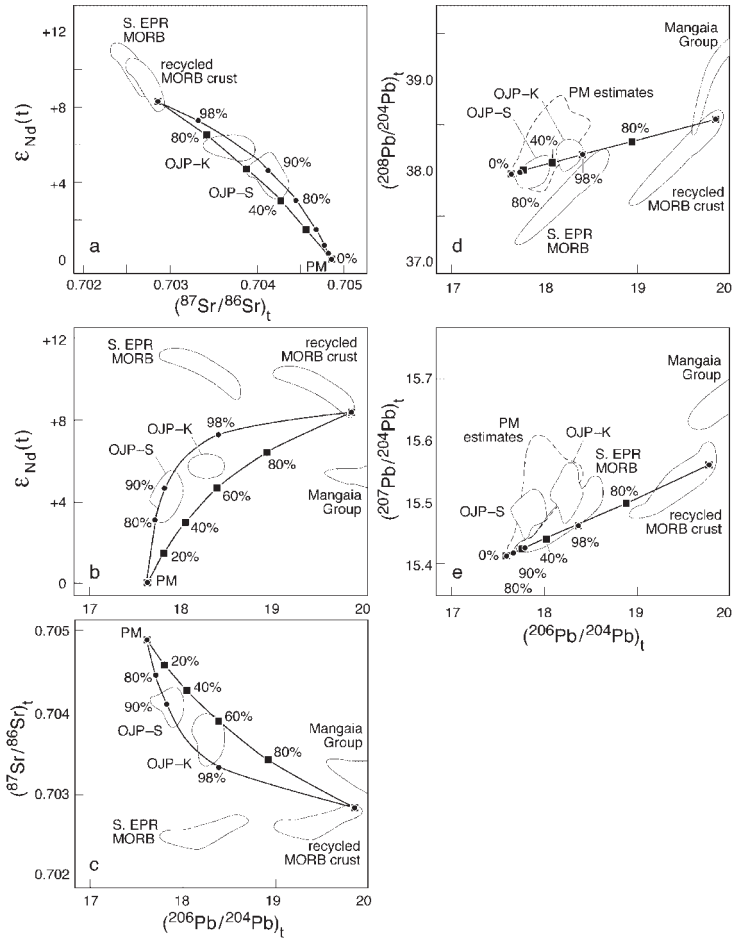

Fig. 11. Example of isotopic mixing curves for two possible combinations of plume peridotite and recycled oceanic upper crust (eclogite) end-members in the OJP mantle source. The plume peridotite is assumed to have primitive mantle compositions and the recycled oceanic crust is assumed to have formed as MORB at 300 Ma from a Pacific MORB-type source, then 'aged' on the seafloor for another 100 my before being subducted, and then to have evolved in the mantle for 80 my before being incorporated into the OJP plume diapir (see Table 6). The concentration and parent–daughter values used are for the less-altered basaltic MORB crust of Kogiso *et al.* (1997). Two extreme cases are illustrated: one case in which the recycled crust melts completely and mixes variably with a 0·5% partial melt from primitive mantle (PM), and the other in which a 100% melt of recycled crust is mixed with a 20% partial melt of primitive mantle in various proportions. The first case indicates that OJP isotopic compositions can be approximated by 80–98% proportions of recycled oceanic crust melt, mixed with very small partial melts of primitive mantle. The second case indicates that if peridotite in the OJP plume mantle is capable of partially melting up to 20%, only 40–60% of recycled oceanic crust is required to explain OJP-type $^{206}Pb/^{204}Pb$, Nd, and Sr isotopic values in the hybrid magmas. Comparable fits also can be achieved by assuming an older age for the recycled MORB end-member. However, all models fail to explain the OJP data fields in the $^{207}Pb/^{204}Pb$ vs $^{206}Pb/^{204}Pb$ diagram, a feature that may be alleviated by choosing a different (yet allowable) primitive-mantle Pb isotope composition [shown as dashed fields in (d) and (e)] or a non-primitive mantle composition. S. EPR MORB, southern East Pacific Rise MORB; OJP-S, OJP Singgalo; OJP-K, OJP Kwaimbaita. Data sources are as in Table 6.

oceanic crust and high proportions of crustal melt in the hybrid magma (~40% or 90–100%, respectively, assuming the plume peridotite partially melts to 20% or 0·5%), as in the isotopic modeling. These proportions are similar to those hypothesized for continental flood basalts by Yasuda *et al.* (1997) from major element considerations.

To estimate the major element compositions of hybrid primary OJP magmas, we used Yasuda *et al.*'s (1997) data on melted MORB (column 1 in Table 7) and results from melting experiments on fertile peridotite KLB-1 (columns 2, 5, and 8 in Table 7; data of Hirose & Kushiro, 1993). Table 7 lists the compositions of hybrid magmas comprising large-degree partial melts (~20%) of fertile peridotite and total melts of recycled upper oceanic crust [taken to be a 100% melt of crust plus 1% peridotite melt, following Yasuda *et al.* (1997); their other hypothetical mixes have higher SiO_2 and Al_2O_3 contents than most OJP lavas]. Proportions of crustal melt in the mixtures shown are 0%, 40%, and 60%, and results for melts in the depth range 2·5, 2·0, and 1·5 GPa are presented. The mixtures show a range of SiO_2, Al_2O_3,

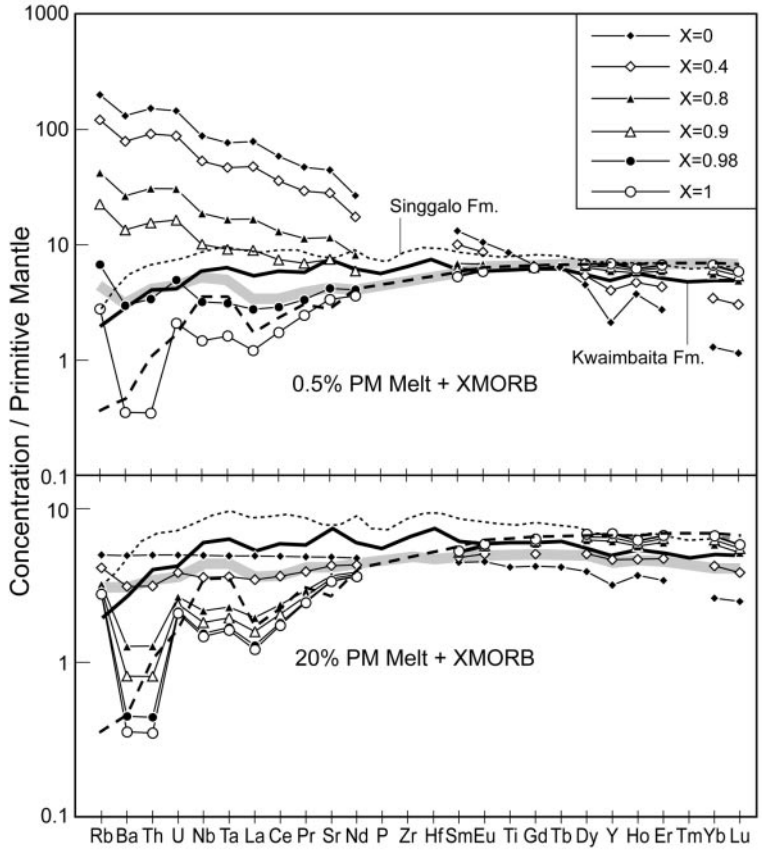

Fig. 12. Calculated primitive-mantle-normalized incompatible element compositions for batch melts of a composite-diapir source containing primitive mantle (PM) and recycled, aged (altered) and dehydrated upper oceanic crust (MORB). Mixing proportions are based on isotopic considerations (see Fig. 11). The patterns with no markers represent the average compositions of Kwaimbaita Fm. (bold filled) and Singgalo Fm. (light dashed) basalts, and average unaltered, but subducted and dehydrated, normal MORB (bold dashed pattern). The top and bottom panels show the trace element patterns produced if a 100% melt of recycled, altered crust is mixed with 0·5% and 20% batch partial melts, respectively, of plume peridotite in various proportions (X values, with $X = 1$ corresponding to no plume peridotite input). The bold filled gray patterns with no markers represent the mixtures involving unaltered, dehydrated MORB that best fit the patterns of OJP lavas [they correspond to $X =$ 0·98 (top panel) and $X = 0{\cdot}40$ (bottom panel)]. Data sources are Mahoney *et al.* (1998) for altered MORB (average of data for DSDP Sites 235 and 245) and Sun & McDonough (1989) for average normal MORB and estimated primitive mantle compositions. The altered and average normal MORB compositions were adjusted to dehydrated compositions using the mobility factors determined by Kogiso *et al.* (1997). Distribution coefficients used are from Arth (1976), Green *et al.* (1989), McKenzie & O'Nions (1991), Hart & Dunn (1993), Kennedy *et al.* (1993), Bedard (1994), the compilation of Green (1994), Hauri *et al.* (1994), Gurenko & Chaussidon (1995), and Xie *et al.* (1995).

TiO_2, and CaO contents, which overlap with those of OJP lavas, except that hybrid primary magmas containing large proportions of peridotite melt have lower Fe_2O_3* and much higher MgO contents (11–13 wt %) than seen for any OJP basalt. The difference in MgO contents can be removed by fractionating the model primary magmas to levels seen in OJP basalts. Fractionation modeling using the 'MELTS' program (Ghiorso & Sack, 1995) is generally consistent with up to 10% fractionation of olivine and spinel, followed by 10–40% removal of clinopyroxene and plagioclase, at pressures varying between ~0·05 and 0·2 GPa (Fig. 13). [An exception is the path calculated for the pure crustal melt of Yasuda *et al.* (1997), which entails up to 15% olivine + feldspar fractionation followed by up to 15% fractionation of the olivine + clinopyroxene + feldspar.] The model fractionation paths, although somewhat lower in Fe_2O_3* and CaO and higher in TiO_2 than the majority of OJP lavas, intersect the OJP range. If such fractionation is considered in the trace element modeling in Fig. 12, the principal effect is to increase the abundances of the incompatible elements. For example, 30% fractionation of an assemblage consisting of 15% clinopyroxene, 75% plagioclase, and 10% olivine leads to a factor of 1·4 and 1·3 increase, respectively, in the abundance of elements with bulk distribution coefficients of 0·04 (e.g. Th, Dy) and 0·20 (e.g. La). This increase slightly improves the concordance of the best-fit model patterns with those of the OJP averages, particularly from Th to Dy. In view of the uncertainties in source composition, fractionation

history, modification of some elemental abundances by post-eruptive alteration, and the ability of the MELTS program to reproduce real-world processes, it appears that melting in a composite diapir may give rise to broadly OJP-type magmas under some conditions.

In summary, we cannot rule out the composite diapir model for the OJP on the basis of isotopic or chemical data alone, given the uncertainties in end-members and in effects of alteration and subduction on oceanic upper crust. A major advantage of this model, relative to the 'simple' plume-head model, is that it does not require an anomalously hot and huge plume head to produce the rate and volume of melting required for continental and oceanic flood basalts. However, in the composite diapir model temperature variations and variations in the distribution of eclogite within the plume head strongly affect the rate and volume of melting, and thus the geochemistry of magmas (Cordery *et al.*, 1997). Yet one of the most outstanding characteristics of the OJP basalts, thus far, is their small overall range of geochemical variation. Furthermore, the stratigraphic succession of Singgalo-type lavas above Kwaimbaita-type lavas is the same in both locations (~1600 km apart) where both lava types have been sampled in a single section. The calculations of Cordery *et al.* (1997) suggest that only the material in the uppermost portion of the plume head will melt significantly. Following Griffiths & Campbell (1990), they assumed the plume head to have a hot cylindrical core (axis) with a thin cap of hot plume-source-dominated material along its upper boundary; the remainder is composed of a cooler mixture of plume-source and entrained lower-mantle material. If so, the Kwaimbaita–Singgalo succession would appear to require an abundance of eclogite within the upper boundary layer, which would melt first to produce the Kwaimbaita-type lavas. Subsequent melting of plume mantle containing a lesser amount of eclogite would produce the Singgalo-type lavas.

One important feature that is difficult to explain with a non-uniform distribution of eclogite within the plume head is the observed abruptness of the change from one isotopically distinct, relatively uniform magma type to another. Also, most of the ~90 Ma OJP basalts studied thus far are isotopically equivalent to the ~122 Ma Kwaimbaita, not Singgalo, lavas, which would require that the plume tail, ~30 my after the initial plateau-forming event, must again contain a high proportion of eclogite, a proportion very similar to that in the upper part of the starting-plume head at ~122 Ma. Yasuda *et al.* (1997) argued that the eclogite is entrained as the rising plume head crosses an eclogite-rich zone near 660 km depth (where eclogite should be neutrally buoyant), which might explain how the upper part of a plume head could contain more recycled oceanic crustal material than the interior. However, the mantle near 660 km crossed by the plume would be expected to contain much less eclogite at ~90 Ma than at ~122 Ma, because much of it would have already been dragged upward by the plume head shortly before ~122 Ma. Finally, if the proportion of eclogite involved in producing OJP magmas was high, as the model suggests, then the plateau's huge size requires a very large amount of recycled oceanic crust to have been concentrated in a relatively small mantle region, so as to become incorporated in a rising plume head. If we assume, for example, that 50×10^6 km^3 of eclogite melted, this value translates to an eclogite layer of 100 km thickness and 399 km in radius; assuming further that such a layer was derived ultimately from the basaltic upper ~2·5 km of the oceanic crust, an immense original area of subducted seafloor (4472 km × 4472 km) is required. In short, it appears that, as with the 'simple' plume-head model, a number of contortions are required for the composite-diapir model to work for the OJP.

OJP's crustal growth and mantle source structure: a synthesis

Crustal growth and structure

Schematic diagrams of possible OJP crustal and mantle source structure during the ~122 Ma event, based on the results of this study and previous geochemical modeling (Mahoney *et al.*, 1993; Tejada *et al.*, 1996; Neal *et al.*, 1997; Tejada, 1998), are shown in Fig. 14. An initial emplacement somewhat off-axis (Mahoney & Spencer, 1991; Coffin & Gahagan, 1995; Gladczenko *et al.*, 1997), and a peridotitic (Fig. 14a) or composite (Fig. 14b) plume head are assumed, despite the first-order discrepancies noted in 'Modeling the OJP's mantle source' between observed features of the OJP and predictions of all current plume-head models. Because of these limitations, the figure should be taken as only a rough working model for future studies. It emphasizes the importance of intrusion, underplating, and cumulate formation (e.g. Neal *et al.*, 1997; Ito & Clift, 1998; Ito & Taira, 2000). Modeling assuming purely peridotite melting suggests that melt generation was polybaric and probably at high potential temperature and initial pressures of at least 4 GPa (Tejada, 1998; and 'Petrogenic implications of chemical variations'); under these conditions, picritic, high-MgO primary melts were probably formed (e.g. Herzberg & Zhang, 1996; Herzberg & O'Hara, 1998). Exposed sections of the much smaller Caribbean Plateau indeed document the existence of picritic lavas at deep crustal levels (e.g. Kerr *et al.*, 1997). The fact that most OJP lavas are relatively Fe-rich basalts, differentiated to roughly similar extents, suggests that primary high-MgO magmas were ponded below the crust or at the Moho (e.g. Cox, 1980; Neal *et al.*, 1997; see Fig. 9). Fractionation of olivine and spinel would decrease the density of the

Table 7: Major element compositions of hypothetical hybrid magmas in a composite diapir source

	100% crust + 1% peridotite melt	KLB-1 2·5 GPa melt $F = 0·20$			KLB-1 2·0 GPa melt $F = 0·22$			KLB-1 1·5 GPa melt $F = 0·19$			OJP lavas
X:	**1·0**	**0**	0·4	0·6	**0**	0·4	0·6	**0**	0·4	0·6	
Melt index (for Fig. 13):	**1% P**		'2.5.4'	'2.5.6'		'2.0.4'	'2.0.6'		'1.5.4'	'1.5.6'	
SiO_2	**49·94**	**47·92**	48·73	49·13	**48·26**	48·94	49·27	**48·72**	49·21	49·45	48·60–50·50
TiO_2	**1·44**	**0·68**	0·99	1·14	**0·51**	0·88	1·07	**0·59**	0·94	1·11	0·90–1·80
Al_2O_3	**15·19**	**13·67**	14·28	14·58	**13·03**	13·89	14·32	**15·05**	15·11	15·13	13·50–15·90
Fe_2O_3*	**10·61**	**9·32**	9·84	10·10	**9·68**	10·05	10·24	**8·31**	9·23	9·69	11·90–15·00
MgO	**8·22**	**15·73**	12·72	11·22	**15·54**	12·61	11·15	**13·00**	11·09	10·13	8·90–6·30
CaO	**11·36**	**10·83**	11·04	11·15	**10·95**	11·11	11·20	**12·18**	11·85	11·68	10·40–13·20
Na_2O	**2·55**	**1·45**	1·89	2·11	**1·36**	1·84	2·07	**1·57**	1·96	2·16	1·48–3·08
K_2O	**0·19**	**0·15**	0·16	0·17	**0·13**	0·15	0·16	**0·08**	0·12	0·14	0·04–0·26
Total	**99·50**	**99·75**	99·65	99·60	**99·46**	99·48	99·48	**99·50**	99·50	99·50	

The columns in bold type represent end-member compositions. *F,* fraction of plume peridotite melting; *X,* fraction of 100% crust + 1% peridotite melt mixture from Yasuda *et al.* (1997) in column 1. Experimental melt compositions are from Hirose & Kushiro (1993). Mixing proportions are based on isotope and trace element modeling results. FeO contents of the experimental and model melts are converted to Fe_2O_3* for comparison with OJP data. Melt index values are labels used in Fig. 13.

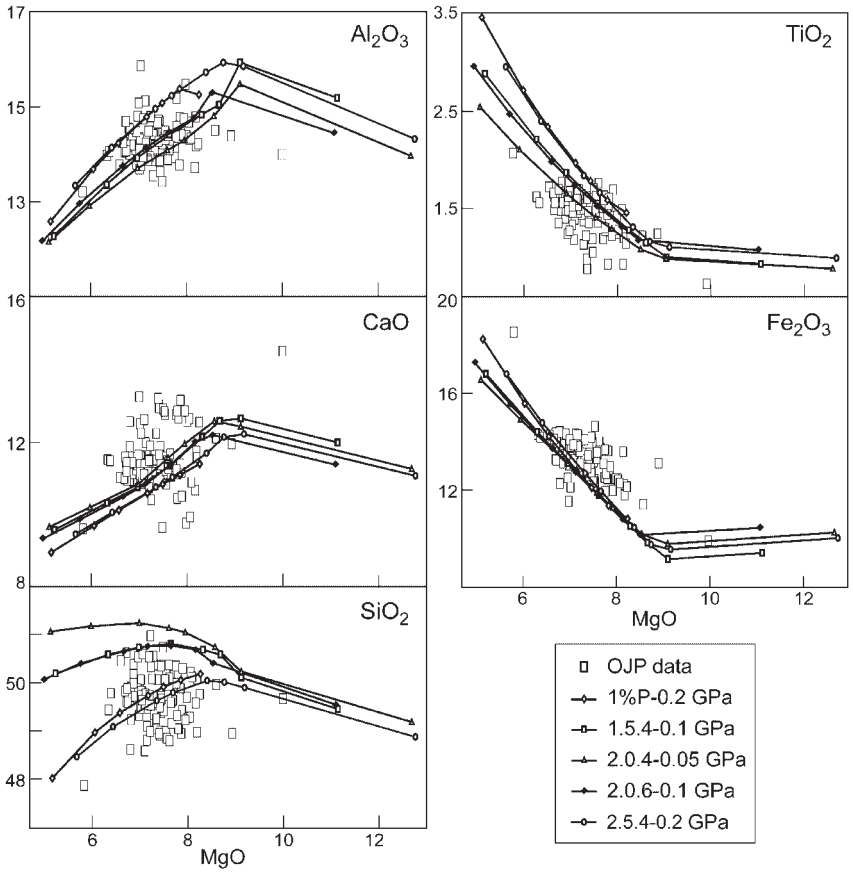

Fig. 13. Major element modeling results for crystal fractionation of mixed crustal eclogite (ex-crust) and peridotite (plume) melts using Ghiorso & Sack's (1995) 'MELTS' program. Parental melt compositions are from Table 7 [e.g. 1% P–0·2 GPa means the melt composition of the 100% crustal + 1% peridotite melt mixture of Yasuda *et al.* (1997) was fractionated at 0·2 GPa]. The markers indicate 10% fractionation intervals. It should be noted that all model runs of the different parental melt compositions at similar pressures of crystallization tend to follow nearly the same liquid lines of descent (LLD) after ~20% fractionation, and thus, for clarity, only a few, representative runs encompassing the full range of results at 0·05 GPa, 0·1 GPa, and 0·2 GPa are shown. The modeling shows that, in a general way, the OJP data may be explained by fractionation at variable depths, consistent with other petrogenetic indicators, such as the phase diagram (Fig. 9), discussed in 'Petrogenetic implications of chemical variations' and suggesting the existence of magma chambers at crustal depths.

melts and enable them to ascend and fractionate further in crustal magma chambers; some magmas undoubtedly froze *en route* in intrusions, whereas some reached the surface, leaving behind more gabbroic cumulates (e.g. Cox, 1980, 1993). The 'hidden cumulates' in the deeper levels of OJP crust probably represent a significant portion of the high-seismic-velocity lower-crustal layer of the plateau (Farnetani *et al.*, 1996; Neal *et al.*, 1997). In a composite diapir scenario, gabbroic cumulates would be less abundant because the hybrid primary magmas would be less Mg rich. The megacrysts and xenoliths in the 'orbicular' basalts in central Malaita described in the section on field characteristics exemplify relatively shallow-level gabbroic cumulates. Also, the high Cl/K ratios of basaltic glasses at Site 807 are suggestive of relatively shallow magma residence because they indicate some shallow-level assimilation of hydrothermally altered crust (Michael, 1999).

Because the portion of the Pacific plate containing the OJP appears to have been near the 125–100 Ma Pacific stage poles and thus drifted little relative to the putative plume (e.g. Neal *et al.*, 1997), Fig. 14 shows vertical to slightly offlapping stacking of ~122 Ma volcanic products. By the time of the Singgalo Fm. eruptions, the earlier volcanic pile and associated cumulates and intrusions had thickened the OJP's crust enormously. This change is reflected in the chemical compositions of Singgalo-type lavas, which appear to represent lower mean fractions of peridotite melting and higher pressures of melt segregation than the Kwaimbaita basalts (Tejada *et al.*, 1996; Neal *et al.*, 1997; Tejada, 1998). In general, lesser total amounts of melting would mean decreased magma

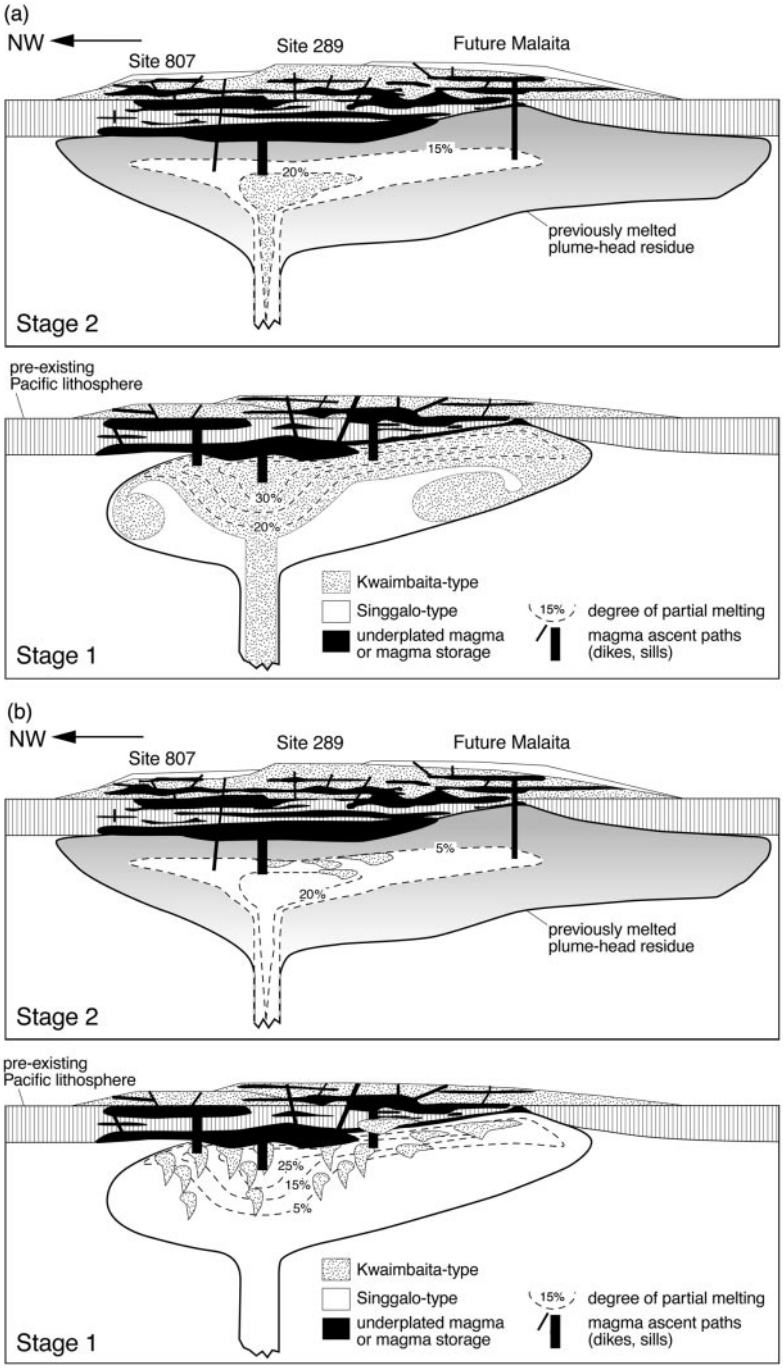

Fig. 14. (a) Schematic crustal and mantle source structure for the OJP, assuming a plume-head origin. Stage 1 (bottom) represents initial ~122 Ma eruption of Kwaimbaita-type lavas fed by melting of the upper portion of the mantle source region, shown as a plume head consisting mainly of plume-source-derived peridotite (e.g. Griffiths & Campbell, 1990). Stage 2 (top) illustrates the subsequent emplacement of Singgalo-type lavas atop Kwaimbaita-type lavas at ~122 Ma. Much of the plume-head mantle has been melted and the melt erupted, intruded into, or underplated to the crust, and the crust has been thickened greatly. Magma chambers are situated at crustal levels and/or near the crust–mantle boundary. The Pacific plate is moving relatively slowly with respect to the mantle source region (Neal *et al.*, 1997). (See text for additional explanation.) (b) Schematic representation of a composite-diapir mantle source for the OJP, with the upper part of the plume head containing most of the entrained eclogite pods, following the Yasuda *et al.* (1997) model. During eruption of Kwaimbaita-type lavas (Stage 1), a greater proportion of the entrained oceanic ex-crustal fragments is required to melt completely and mix with partial melts of the peridotite plume matrix. At the time of eruption of Singgalo-type lavas (Stage 2) the few eclogitic fragments remaining melt completely and mix with partial melts of the peridotite matrix. (See text.)

supply to magma chambers, possibly leading to slightly higher amounts of fractionation, on average, as inferred for the Singgalo Fm. (relative to the Kwaimbaita). Overall, although the crust of the OJP is much thicker (30–43 km; e.g. Miura *et al.*, 1996; Gladczenko *et al.*, 1997; Richardson *et al.*, 2000) than that of the Caribbean Plateau (<20 km; Mauffret & Leroy, 1999), the gross crustal structure of the Caribbean and the Ontong Java Plateaux may be rather similar (e.g. Hussong *et al.*, 1979; Kerr *et al.*, 1997; Phinney *et al.*, 1999).

Compositional structure of mantle source region

The time difference between emplacement of the Kwaimbaita and the Singgalo basalts is beyond the resolution of current ^{40}Ar–^{39}Ar dating capabilities, given the low K_2O contents of most OJP basement rocks [but may just be distinguishable at Site 807 when biostratigraphic data are taken into account; see Larson & Erba (1999)]. Stratigraphically, the change in isotopic compositions is abrupt, and implies a source with two distinct compositional regions and probably a component of vertical stratification.

In Griffiths & Campbell's (1990) model, hot plume-source-derived material (light gray shading in Fig. 14a) is carried to the stagnation point at the cap of the plume and spreads laterally into thin laminae. In a broad area around the center of the head, plume-source-dominated peridotite lies above a region enriched in entrained peridotite (white in Fig. 14a). In this context, the Kwaimbaita and Singgalo basalts can be interpreted as corresponding, respectively, to the upper, plume-source-dominated zone and the underlying zone containing more entrained material. Griffiths & Campbell (1990) also argued that for a very large plume head, of which the OJP case is one of the two most viable examples, little entrainment of non-plume mantle would occur because the plume head would ascend too rapidly. For this reason, the amount of plume-source material depicted in Fig. 14a is much greater than that of entrained mantle. Furthermore, Van Keken's (1998) numerical simulation indicated that much of the plume-source material would be contained in the plume head and that the trailing conduit at this stage would be composed largely of entrained non-plume mantle. Thus, Fig. 14a shows a reduced amount of plume-source material at greater depth and tapping of mostly entrained mantle in the later stages of ~122 Ma volcanism. In Yasuda *et al.*'s (1997) composite diapir model, the upper part of the plume head contains most of the eclogite pods, and Fig. 14b shows most of them melting completely and mixing with partial melts of the peridotite matrix during the eruption of the Kwaimbaita basalts (Stage 1). At the time of the Singgalo eruptions (Stage 2) fewer entrained eclogitic fragments remain, resulting in a decreased contribution of melt derived from subducted oceanic crust to the total melt.

CONCLUSIONS

(1) Geochemical and geochronological study of 0·5 and 3·5 km sections of pillowed and massive basaltic flows composing crustal basement in central Malaita reveals a sequence of 123·1 ± 1·4 Ma OJP crust resembling a greatly expanded section of that at ODP Site 807. The results further confirm the importance of a major ~122 Ma eruptive episode and a nearly plateau-wide distribution of two isotopically distinct types of basalt in the world's largest oceanic plateau.

(2) As at Site 807, the two types of basalt form stratigraphically separate groups. With the Kwaio Anticline as the type locality, we term the stratigraphically lower group (maximum thickness >2·7 km) the Kwaimbaita Fm. and the overlying group (maximum exposed thickness of 750 m in central Malaita) the Singgalo Fm. On the basis of closely similar isotopic and elemental characteristics, this nomenclature is extended to other locations where ~122 Ma OJP basement has been sampled, including northeastern Santa Isabel, Ramos Island, southern Malaita, ODP Site 807, and DSDP Site 289. The Singgalo magma type appears to be much more voluminous in the south than in the northern plateau (e.g. only 46 m of flows at Site 807 and none at Site 289).

(3) Isotopic variation within each group is very limited and indicates an isotopically ocean-island-type mantle source with two distinct compositional regions, each of which was fairly homogeneous relative to the scale of melting. No evidence of normal-MORB-type mantle is present. The sharp stratigraphic boundary between the Kwaimbaita and Singgalo formations in Malaita and, ~1600 km away, between the two corresponding groups at Site 807, coupled with the apparent lack of translational motion of this part of the Pacific plate between 125 and 100 Ma, suggests a vertically stratified structure for the OJP source mantle.

(4) The ocean-island-like isotopic signatures of OJP lavas can be accommodated with either a peridotite plume head (whether originating above a thermal boundary layer or at mid-mantle depths) or a composite diapir model, in which a dominantly peridotitic plume head is assumed to contain pockets of eclogite. Both models may also accommodate the major and trace element data, although the compositions of model melts of a mixed eclogite–peridotite source provide only rough fits to the OJP data. Better fits are obtained assuming a two-component peridotitic source (Mahoney *et al.*, 1993; Tejada *et al.*, 1996; Neal *et al.*, 1997; Tejada, 1998). The composite diapir model also requires an enormous

amount of eclogite to have been concentrated in a relatively small part of the mantle if OJP magmas are assumed to comprise a significant proportion of eclogite melt. Furthermore, the abrupt transition from Kwaimbaita- to Singgalo-type basalts, and the reappearance some 30 my later of Kwaimbaita-like lavas are not readily explained by the composite diapir model.

(5) In several important respects, the OJP fails to fit the predictions of, and thus poses a challenge to, any plume-head model: the absence of evidence for significant uplift despite construction of a crust of ~35 km thickness during what should have been the impact of the largest plume head in the last 200 my, the lack of an attached seamount chain (plume-tail trace), and the presence of at least two important episodes of eruptive activity separated in time by ~30 my.

ACKNOWLEDGEMENTS

We thank T. Babbs and A. Saunders for allowing us to use their unpublished data, R. Magu for providing his field and petrographic notes, L. Kroenke, M. Garcia, J. Sinton, A. Pietruszka, and G. Fitton for helpful discussions, K. Spencer, K. Rubin, T. Hulsebosch, and J. C. Jain for help with the analytical work, and N. Hulbirt for improving the figures. Ian Parkinson and an anonymous reviewer provided valuable critical reviews. The Solomon Islands Ministry of Energy, Water, and Mineral Resources (Geology Mapping) provided invaluable logistical support, enthusiastic guidance, and diplomacy in the bush. This study was supported by NSF-EAR grants to J.J.M., C.R.N., and R.A.D., and a Faculty Development Grant from the University of the Philippines to M.L.G.T.

REFERENCES

Anderson, D. L. (1996). Enriched asthenosphere and depleted plumes. *International Geology Reviews* **38**, 1–21.

Anderson, D. L., Zhang, Y.-S. & Tanimoto, T. (1992). Plume heads, continental lithosphere, flood basalts, and tomography. In: Storey, B., Alabaster, T. & Pankhurst, R. J. (eds) *Magmatism and Causes of Continental Break-up*. *Geological Society, London, Special Publications* **68**, 99–124.

Arth, J. G. (1976). Behavior of trace elements during magmatic processes—a summary of theoretical models and their applications. *Journal of Research and Geological Survey* **4**, 41–47.

Babbs, T. L. (1997). Geochemical and petrological investigations of the deeper portions of the Ontong Java Plateau: Malaita, Solomon Islands. Ph.D. dissertation, Leicester University, 254 pp.

Barron, A. J. M. (1993). *The Geology of Northernmost Malaita: a Description of Sheets 8/160/7 and 8/150/8*. Geological Division Report. Honiara: Solomon Islands Ministry of Natural Resources, 42 pp.

Bedard, J. H. (1994). A procedure for calculating the equilibrium distribution of trace elements among the minerals of cumulate rocks, and the concentration of trace elements among the minerals of cumulate rocks, and the concentration of trace elements in the coexisting liquids. *Chemical Geology* **118**, 143–153.

Berger, W. H., Kroenke, L. W., Mayer, L. A., *et al.* (eds) (1993). *Proceedings of the Ocean Drilling Program, Scientific Results, 130*. College Station, TX: Ocean Drilling Program.

Bienvenu, P., Bougault, H., Joron, J. L., Treuil, M. & Dmitriev, L. (1990). MORB alteration: rare-earth element/non-rare-earth hygromagmaphile element fractionation. *Chemical Geology* **82**, 1–14.

Birkhold-VanDyke, A. L., Neal, C. R., Jain, J. C., Mahoney, J. J. & Duncan, R. A. (1996). Multi-stage growth for the Ontong Java Plateau (OJP)? A progress report from San Cristobal (Makira), Solomon Islands. *EOS Transactions, American Geophysical Union* **77**, F714.

Castillo, P., Pringle, M. S. & Carlson, R. W. (1994). East Mariana Basin tholeiites: Jurassic ocean crust or Cretaceous rift basalts related to the Ontong Java plume? *Earth and Planetary Science Letters* **123**, 139–154.

Chauvel, C., Hoffman, A. W. & Vidal, P. (1992). HIMU-EM: the French Polynesian connection. *Earth and Planetary Science Letters* **110**, 99–119.

Chen, C.-Y., Frey, F. A., Rhodes, J. M. & Easton, R. M. (1996). Temporal geochemical evolution of Kilauea volcano: comparison of Hilina and Puna basalt. In: Basu, A. R. & Hart, S. (eds) *Earth Processes: Reading the Isotopic Code. Geophysical Monograph, American Geophysical Union* **95**, 161–181.

Coffin, M. F. & Eldholm, O. (1994). Large igneous provinces: crustal structure, dimensions, and external consequences. *Reviews of Geophysics* **32**, 1–36.

Coffin, M. F. & Gahagan, L. M. (1995). Ontong Java and Kerguelen Plateaux: Cretaceous Icelands? *Journal of the Geological Society, London* **152**, 1047–1052.

Coleman, P. J. & Kroenke, L. W. (1981). Subduction without volcanism in the Solomon Islands Arc. *Geo-Marine Letters* **1**, 129–134.

Coleman, P. J., McGowran, B. & Ramsay, W. R. H. (1978). New, Early Tertiary ages for basal pelagites, Northeastern Santa Isabel, Solomon Islands (central southwest flank, Ontong Java Plateau). *Bulletin of the Australian Society of Exploration Geophysicists* **9**(3), 110–114.

Cordery, M. J., Davies, G. F. & Campbell, I. H. (1997). Genesis of flood basalts from eclogite-bearing mantle plumes. *Journal of Geophysical Research* **102**, 20179–20197.

Cox, K. G. (1980). A model for flood basalt vulcanism. *Journal of Petrology* **21**, 629–650.

Cox, K. G. (1993). Continental magmatic underplating. *Philosophical Transactions of the Royal Society of London, Series A* **342**, 155–166.

Cserepes, L. & Yuen, D. A. (2000). On the possibility of a second kind of mantle plume. *Earth and Planetary Science Letters* **183**, 61–71.

Davis, G. L. (1978). Zircons from the mantle. *US Geological Survey Open File Report* **78-701**, 86–88.

Duncan, R. A., Hooper, P. R., Rehacek, J., Marsh, J. S. & Duncan, A. R. (1997). The timing and duration of the Karoo igneous event, southern Gondwana. *Journal of Geophysical Research* **102**, 18127–18138.

Farnetani, C. G., Richards, M. A. & Ghiorso, M. S. (1996). Petrological models of magma evolution and deep crustal structure beneath hotspots and flood basalt provinces. *Earth and Planetary Science Letters* **143**, 81–96.

Galer, S. J. G. & Goldstein, S. L. (1996). Influence of accretion on lead in the earth. In: Basu, A. R. & Hart, S. (eds) *Earth Processes: Reading the Isotopic Code. Geophysical Monograph, American Geophysical Union* **95**, 75–98.

Garcia, M. O., Foss, D. J., West, H. B. & Mahoney, J. J. (1995). Geochemical and isotopic evolution of Loihi volcano, Hawaii. *Journal of Petrology* **36**(6), 1647–1674.

Garcia, M. O., Rhodes, J. M., Trusdell, F. A. & Pietruszka, A. J. (1996). Petrology of lavas from Puu Oo eruption of Kilauea volcano: III. The Kupaianaha episode (1986–1992). *Bulletin of Volcanology* **58**, 359–379.

Ghiorso, M. S. & Sack, R. O. (1995). Chemical mass transfer in magmatic processes, IV. A revised and internally consistent thermodynamic model for the interpolation and extrapolation of liquid–solid equilibria in magmatic systems at elevated temperatures and pressure. *Contributions to Mineralogy and Petrology* **119**, 197–212.

Gladczenko, T. P., Coffin, M. F. & Eldholm, O. (1997). Crustal structure of the Ontong Java Plateau: modeling of new gravity and existing seismic data. *Journal of Geophysical Research* **102**, 22711–22729.

Govindaraju, K. (1994). 1994 Compilation of working values and sample descriptions for 383 geostandards. *Geostandards Newsletter, Special Issue* **18**, 15–16.

Green, T. H. (1994). Experimental studies of trace-element partitioning applicable to igneous petrogenesis—Sedona 16 years later. *Chemical Geology* **117**, 1–36.

Green, T. H., Sie, S. H., Ryan, C. G. & Cousens, D. R. (1989). Proton microprobe-determined partitioning of Nb, Ta, Zr, Sr, and Y between garnet, clinopyroxene and basaltic magma at high pressure and temperature. *Chemical Geology* **74**, 210–216.

Griffiths, R. W. & Campbell, I. H. (1990). Stirring and structure in mantle starting plumes. *Earth and Planetary Science Letters* **99**, 66–78.

Grove, T. L., Kinzler, R. J. & Bryan, W. B. (1992). Fractionation of mid-ocean ridge basalt (MORB). In: Phipps Morgan, J., Blackman, D. K. & Sinton, J. (eds) *Mantle Flow and Melt Generation at Mid-Ocean Ridges. Geophysical Monograph, American Geophysical Union* **71**, 281–310.

Gurenko, A. A. & Chaussidon, M. (1995). Enriched and depleted primitive melts included in olivine from Icelandic tholeiites: origin by continuous melting of a single mantle column. *Geochimica et Cosmochimica Acta* **58**, 2905–2917.

Hart, S. R. & Dunn, T. (1993). Experimental cpx/melt partitioning of 24 trace elements. *Contributions to Mineralogy and Petrology* **113**, 1–8.

Hauri, E. H., Wagner, T. & Grove, T. L. (1994). Experimental partitioning of Th, U, Pb and other trace elements between garnet, clinopyroxene and basaltic melts. *Chemical Geology* **117**, 149–166.

Hawkins, M. P. & Barron, J. M. (1991). *The Geology and Mineral Resources of Santa Isabel. Geological Division Report* J25. Honiara: Solomon Islands Ministry of Natural Resources, 114 pp.

Herzberg, C. & O'Hara, M. J. (1998). Phase equilibrium constraints on the origin of basalts, picrites, and komatiites. *Earth-Science Reviews* **44**, 39–79.

Herzberg, C. & Zhang, J. (1996). Melting experiments on anhydrous peridotite KLB-1: compositions of magmas in the upper mantle and transition zone. *Journal of Geophysical Research* **101**, 8271–8295.

Hirose, H. & Kushiro, I. (1993). Partial melting of dry peridotites at high pressures: determination of compositions of melts segregated from peridotite using aggregates of diamond. *Earth and Planetary Science Letters* **114**, 477–489.

Hughes, G. W. & Turner, C. C. (1976). *Geology of Southern Malaita.* Geological Survey Division, Bulletin 2. Honiara: Solomon Islands Ministry of Natural Resources, 80 pp.

Hughes, G. W. & Turner, C. C. (1977). Upraised Pacific Ocean floor, southern Malaita, Solomon Islands. *Geological Society of America Bulletin* **88**, 412–424.

Hussong, D. M., Wipperman, L. K. & Kroenke, L. W. (1979). The crustal structure of the Ontong Java and Manihiki oceanic plateaus. *Journal of Geophysical Research* **84**, 6003–6010.

Ito, G. T. & Clift, P. D. (1998). Subsidence and growth of Pacific Cretaceous plateaus. *Earth and Planetary Science Letters* **161**, 85–100.

Ito, G. T. & Taira, A. (2000). Compensation of the Ontong Java Plateau by surface and subsurface loading. *Journal of Geophysical Research* **105**, 11171–11183.

Jacobsen, S. B. & Wasserburg, G. J. (1980). Sm–Nd isotopic evolution of chondrites. *Earth and Planetary Science Letters* **50**, 139–155.

Jain, J. C. & Neal, C. R. (1996). Report of the inductively coupled plasma-mass spectrometry (ICP-MS) facility, University of Notre Dame 1993–1996. Open File Report, University of Notre Dame, 30 pp.

Jenner, G. A., Longerich, H. P., Jackson, S. E. & Fryer, B. J. (1990). ICP-MS—a powerful tool for high precision trace element analysis in earth sciences: evidence from analysis of selected U.S.G.S. reference samples. *Chemical Geology* **83**, 133–148.

Kennedy, A. K., Lofgren, G. E. & Wasserburg, G. J. (1993). An experimental study of trace element partitioning between olivine, orthopyroxene, and melt in chondrules: equilibrium values and kinetic effects. *Earth and Planetary Science Letters* **115**, 177–195.

Kerr, A. C., Tarney, J., Marriner, G. F., Nivia, A. & Saunders, A. D. (1997). The Caribbean–Colombian Cretaceous igneous province: the internal anatomy of an oceanic plateau. In: Mahoney, J. J. & Coffin, M. F. (eds) *Large Igneous Provinces: Continental, Oceanic, and Planetary Flood Volcanism. Geophysical Monograph, American Geophysical Union* **100**, 123–144.

Kogiso, T., Tatsumi, Y. & Nakano, S. (1997). Trace element transport during dehydration processes in the subducted oceanic crust: 1. Experiments and implications for the origin of ocean island basalts. *Earth and Planetary Science Letters* **148**, 193–205.

Kroenke, L. W. (1972). *Geology of the Ontong Java Plateau. Hawaii Institute of Geophysics, Report 72-75.* Honolulu: University of Hawaii, 119 pp.

Kurz, M. D., Kenna, T., Kammer, D., Rhodes, J. M. & Garcia, M. O. (1995). Isotopic evolution of Mauna Loa volcano: a view from the submarine southwest rift zone. In: Rhodes, J. M. & Lockwood, J. P. (eds) *Mauna Loa Revealed: Structure, Composition, History, and Hazards. Geophysical Monograph, American Geophysical Union* **92**, 45–80.

Lanphere, M. A., Dalrymple, G. B., Fleck, R. S. & Pringle, M. S. (1990). Intercalibration of mineral standards for K–Ar and ^{40}Ar–^{39}Ar age measurements. *EOS Transactions, American Geophysical Union* **71**, 1658.

Larson, R. L. & Erba, E. (1999). Onset of mid-Cretaceous greenhouse in the Barremian–Aptian: igneous events and the biological, sedimentary, and geochemical consequences. *Paleoceanography* **14**, 663–678.

Libourel, G., Boivin, P. & Biggar, G. M. (1989). The univariant curve liquid = forsterite + anorthite + diopside in the system CMAS at 1 bar: solid solutions and melt structure. *Contributions to Mineralogy and Petrology* **102**, 406–421.

Longhi, J. (1987). Liquidus equilibria and solid solution in the system $CaAl_2Si_2O_8$–Mg_2SiO_4–$CaSiO_3$–SiO_2 at low pressure. *American Journal of Science* **287**, 265–331.

Mahoney, J. J. (1987). An isotopic survey of Pacific oceanic plateaus: implications for their nature and origin. In: Keating, B., Fryer, P., Batiza, R. & Boehlert, G. (eds) *Seamounts, Islands, and Atolls. Geophysical Monograph, American Geophysical Union* **43**, 207–220.

Mahoney, J. J. & Spencer, K. J. (1991). Isotopic evidence for the origin of the Manihiki and Ontong Java oceanic plateaus. *Earth and Planetary Science Letters* **104**, 196–210.

Mahoney, J. J., Storey, M., Duncan, R. A., Spencer, K. J. & Pringle, M. (1993). Geochemisty and geochronology of the Ontong Java Plateau. In: Pringle, M., Sager, W., Sliter, W. & Stein, S. (eds) *The Mesozoic Pacific. Geology, Tectonics, and Volcanism. Geophysical Monograph, American Geophysical Union* **77**, 233–261.

Mahoney, J. J., Sinton, J. M., Kurz, M. D., MacDougall, J. D., Spencer, K. J. & Lugmair, G. W. (1994). Isotope and trace element characteristics of a super-fast spreading ridge: East Pacific Rise, 13–23°S. *Earth and Planetary Science Letters* **121**, 173–193.

Mahoney, J. J., Frei, R., Tejada, M. L. G., Mo, X. X., Leat, P. T. & Nägler, T. F. (1998). Tracing the Indian Ocean mantle domain through time: isotopic results from old West Indian, East Tethyan, and South Pacific seafloor. *Journal of Petrology* **39**, 1285–1306.

Mahoney, J. J., Fitton, J. G., Wallace, P. J., *et al.* (eds) (2002). *Proceedings of the Ocean Drilling Program, Initial Reports, 192*. College Station, TX: Ocean Drilling Program, in press.

Mauffret, A. & Leroy, S. (1999). Seismic stratigraphy and structure of the Caribbean igneous province. *Tectonophysics* **283**, 61–104.

Michael, P. J. (1999). Implications for magmatic processes at Ontong Java Plateau from volatile and major element contents of Cretaceous basalt glasses. *Geochemistry, Geophysics, Geosystems* **1**, paper no. 1999GC000025 [10 170 words, 6 figures, 2 tables].

Miura, S., Shinohara, M., Takahashi, N., Araki, E., Taira, A., Suyehiro, K., Coffin, M. F., Shipley, T. & Mann, P. (1996). OBS crustal structure of the Ontong Java Plateau converging into Solomon island arc (abstract). *EOS Transactions, American Geophysical Union*, **77F**, 713.

McCulloch, M. T. & Black, L. P. (1984). Sm–Nd isotopic systematics of Enderby Land granulites and evidence for the redistribution of Sm and Nd during metamorphism. *Earth and Planetary Science Letters* **71**, 46–58.

McDonough, W. F. & Sun, S.-s. (1995). The composition of the Earth. *Chemical Geology* **120**, 223–253.

McGinnis, C. E., Jain, J. C. & Neal, C. R. (1997). Characterization of memory effects and development of an effective wash protocol for the measurement of petrogenetically critical trace elements in geological samples by ICP-MS. *Geostandards Newsletter* **21**, 289–305.

McKenzie, D. & O'Nions, R. K. (1991). Partial melt distributions from inversion of rare earth element concentrations. *Journal of Petrology* **32**, 1021–1091.

Moore, J. G., Normark, W. R. & Szabo, B. J. (1990). Reef growth and volcanism on the submarine southwest rift zone of Mauna Loa, Hawaii. *Bulletin of Volcanology* **52**, 375–380.

Nakamura, Y. & Tatsumoto, M. (1988). Pb, Nd, and Sr isotopic evidence for a multicomponent source for rocks of Cook–Austral Island and heterogeneities of mantle plumes. *Geochimica et Cosmochimica Acta* **52**, 2909–2924.

Neal, C. R., Mahoney, J. J., Kroenke, L. W., Duncan, R. A. & Petterson, M. G. (1997). The Ontong Java Plateau. In: Mahoney, J. J. & Coffin, M. F. (eds) *Large Igneous Provinces: Continental, Oceanic, and Planetary Flood Volcanism. Geophysical Monograph, American Geophysical Union* **100**, 183–216.

Norrish, K. & Chappell, B. W. (1977). X-ray fluorescence spectrometry. In: Zussman, J. (ed.) *Physical Methods in Determinative Mineralogy*. New York: Academic Press, pp. 201–272.

Palacz, Z. & Saunders, A. D. (1986). Coupled trace element isotope enrichment on the Cook–Austral–Samoa Islands, southwest Pacific. *Earth and Planetary Science Letters* **79**, 270–280.

Parkinson, I. J., Arculus, R. J. & Duncan, R. A. (1996). Geochemistry of Ontong Java Plateau basalt and gabbro sequences, Santa Isabel, Solomon Islands. *EOS Transactions, American Geophysical Union* **77**, F715.

Peng, Z. X. & Mahoney, J. J. (1995). Drillhole lavas from the northwestern Deccan Traps, and the evolution of Reunion hotspot mantle. *Earth and Planetary Science Letters* **134**, 169–185.

Petterson, M. G. (1995). *The Geology of North and Central Malaita, Solomon Islands (Including Implications of Geological Research on Makira, Savo Island, Guadalcanal, and Choiseul between 1992 and 1995)*. Water and Mineral Resources Division Geological Memoir 1/95. Honiara: Solomon Islands Ministry of Energy, Water, and Mineral Resources.

Petterson, M. G., Neal, C. R., Mahoney, J. J., Kroenke, L. W., Saunders, A. D., Babbs, T. L., Duncan, R. A., Tolia, D., McGrail, B. & Barron, M. (1997). Structure and deformation of north and central Malaita, Solomon Islands: tectonic implications for the Ontong Java Plateau–Solomon Arc collision, and for the fate of oceanic plateaus. *Tectonophysics* **283**, 1–33.

Phinney, E. J., Mann, P., Coffin, M. F. & Shipley, T. H. (1999). Sequence stratigraphy, structure, and tectonic history of the southwestern Ontong Java Plateau adjacent to the North Solomon Trench and Solomon Islands arc. *Journal of Geophysical Research* **104**, 20449–20466.

Rhodes, J. M. & Hart, S. R. (1995). Evolution of Mauna Loa volcano: episodic trace element and isotopic variations in historical Mauna Loa lavas: implications for magma and plume dynamics. In: Rhodes, J. M. & Lockwood, J. P. (eds) *Mauna Loa Revealed: Structure, Composition, History, and Hazards. Geophysical Monograph, American Geophysical Union* **92**, 263–288.

Richards, M. A., Duncan, R. A. & Courtillot, V. (1989). Flood basalts and hot-spot tracks: plume heads and tails. *Science* **246**, 103–107.

Richardson, W. P., Okal, E. A. & Van der Lee, S. (2000). Rayleigh-wave tomography of the Ontong Java Plateau. *Physics of the Earth and Planetary Interiors* **118**, 29–51.

Rickwood, F. K. (1957). Geology of the island of Malaita. In: *Geological Reconnaissance of Parts of the Central Islands of B.S.I.P. Colonial Geology and Mineral Resources* **6** (3), 300–306.

Roden, M. F., Trull, T., Hart, S. R. & Frey, F. A. (1994). New He, Nd, Pb, and Sr isotopic constraints on the constitution of the Hawaiian plume: results from Koolau Volcano, Oahu, Hawaii, USA. *Geochimica et Cosmochimica Acta* **58**(5), 1431–1440.

Sager, W. W. & Han, H.-C. (1993). Rapid formation of the Shatsky Rise oceanic plateau inferred from its magnetic anomaly. *Nature* **364**, 610–613.

Sheth, H. C. (1999). Flood basalts and large igneous provinces from deep mantle plumes: fact, fiction, and fallacy. *Tectonophysics* **311**, 1–29.

Smith, A. D. & Lewis, C. (1999). The planet beyond the plume hypothesis. *Earth-Science Reviews* **48**, 135–182.

Smith, W. H. F. & Sandwell, D. T. (1996). New global seafloor topography from satellite altimetry. *EOS Transactions, American Geophysical Union* **77**, F315.

Stille, P., Unruh, D. M. & Tatsumoto, M. (1983). Pb, Sr, Nd, and Hf isotopic evidence of multiple sources for Oahu, Hawaii basalts. *Nature* **304**, 25–29.

Sun, S.-S. & McDonough, W. F. (1989). Chemical and isotopic systematics of oceanic basalts: implications for mantle composition and processes. In: Saunders, A. D. & Norry, M. J. (eds) *Magmatism in the Ocean Basins. Geological Society, London, Special Publications* **42**, 313–345.

Tarduno, J. A., Sliter, W. V., Kroenke, L. W., Leckie, M., Mahoney, J. J., Musgrave, R. J., Storey, M. & Winterer, E. L. (1991). Rapid formation of the Ontong Java Plateau by Aptian mantle plume volcanism. *Science* **254**, 399–403.

Tatsumoto, M. (1978). Isotopic composition of lead in oceanic basalt and its implication to mantle evolution. *Earth and Planetary Science Letters* **38**, 63–87.

Tejada, M. L. G. (1998). Geochemical studies of Pacific oceanic plateaus: the Ontong Java Plateau and Shatsky Rise. Ph.D. dissertation, University of Hawaii, Honolulu, 328 pp.

Tejada, M. L. G., Mahoney, J. J., Duncan, R. A. & Hawkins, M. P. (1996). Age and geochemistry of basement and alkalic rocks of Malaita and Santa Isabel, Solomon Islands, southern margin of Ontong Java Plateau. *Journal of Petrology* **37**(2), 361–394.

Todt, W., Cliff, R. A., Hanser, A. & Hoffman, A. W. (1996). Evaluation of a ^{202}Pb–^{205}Pb double spike for high-precision lead isotope analysis. In: Basu, A. & Hart, S. (eds) *Earth Processes: Reading the Isotopic Code. Geophysical Monograph, American Geophysical Union* **95**, 429–437.

Van Keken, P. (1998). Evolution of starting mantle plumes: a comparison between numerical and laboratory models. *Earth and Planetary Science Letters* **148**, 1–11.

Vidal, P., Chauvel, C. & Brousse, R. (1984). Large mantle heterogeneity beneath French Polynesia. *Nature* **307**, 536–538.

Walter, M. J. & Presnall, D. C. (1994). Melting behavior of simplified lherzolite in the system CaO–MgO–Al_2O_3–SiO_2–Na_2O from 7 to 35 kbar. *Journal of Petrology* **35**, 329–359.

White, R. S. (1993). Melt production rates in mantle plumes. *Philosophical Transactions of the Royal Society of London* **342**, 137–153.

White, W. M. (1993). $^{238}U/^{204}Pb$ in MORB and open system evolution of the depleted mantle. *Earth and Planetary Science Letters* **115**, 211–226.

Xie, Q., McCuaig, T. C. & Kerrich, R. (1995). Secular trends in the melting depth of mantle plumes: evidence from HFSE/REE systematics of Archean high-Mg lavas and modern oceanic basalts. *Chemical Geology* **126**, 29–42.

Yasuda, A., Fujii, T. & Kurita, K. (1997). A composite diapir model for extensive basaltic volcanism: magmas from subducted oceanic crust entrained within mantle plumes. *Proceedings of the Japan Academy* **73**(10), 201–204.